Quantum Chemical and Master Equation Studies of the Methyl Vinyl Carbonyl Oxides Formed in Isoprene Ozonolysis

Keith T. Kuwata,* Lukas C. Valin, and Amber D. Converse

Department of Chemistry, Macalester College, Saint Paul, Minnesota 55105-1899

Received: August 4, 2005; In Final Form: October 3, 2005

Methyl vinyl carbonyl oxide is an important intermediate in the reaction of isoprene and ozone and may be responsible for most of the •OH formed in isoprene ozonolysis. We use CBS-QB3 calculations and RRKM/master equation simulations to characterize all the pathways leading to the formation of this species, all the interconversions among its four possible conformers, and all of its irreversible isomerizations. Our calculations, like previous studies, predict •OH yields consistent with experiment if thermalized *syn*-methyl carbonyl oxides form •OH quantitatively. Natural bond order analysis reveals that the vinyl group weakens the C=O bond of the carbonyl oxide, making rotation about this bond accessible to this chemically activated intermediate. The vinyl group also allows one conformer of the carbonyl oxide to undergo electrocyclization to form a dioxole, a species not previously considered in the literature. Dioxole formation, which has a CBS-QB3 reaction barrier of 13.9 kcal/mol, is predicted to be favored over vinyl hydroperoxide formation, dioxirane formation, and collisional stabilization. Our calculations also predict that two dioxole derivatives, 1,2-epoxy-3-butanone and 3-oxobutanal, should be major products of isoprene ozonolysis.

I. Introduction

Isoprene (2-methyl-1,3-butadiene) is one of the most abundant volatile organic compounds in the troposphere, with global emissions estimated at 5×10^{14} g C per year.[1] The predominant loss pathways for isoprene, like all alkenes, are reactions with hydroxyl radical (•OH), nitrate radical (•NO$_3$), and ozone (O$_3$).[2−4] Although isoprene's lifetime with respect to the O$_3$ reaction is ~20 times longer than that with respect to the •OH or •NO$_3$ reactions,[3,4] the isoprene−O$_3$ reaction has particular atmospheric significance in that it generates •OH nonphotochemically.[5−10] The ozonolysis of isoprene can therefore be the dominant source of tropospheric •OH both at night and over heavily forested areas.[5]

According to the Criegee mechanism (Scheme 1), isoprene ozonolysis starts with the concerted cycloaddition of ozone to one of the double bonds of isoprene, forming the 1,2-primary ozonide (or 4-methyl-4-vinyl-1,2,3-trioxolane, **4**) and the 3,4-primary ozonide (or 4-(2-propenyl)-1,2,3-trioxolane, **4'**). The ozonides then undergo concerted cycloreversion to form formaldehyde (**6**), methyl vinyl ketone (or MVK, **9**), methacrolein (**9'**), and a variety of carbonyl oxides (or Criegee intermediates, **7**, **7'**, and **8**).

Since the initial reports of •OH formation in gas-phase isoprene ozonolysis, the mechanistic challenge has been to identify the specific •OH precursors. On the basis of experimental measurements of product yields, Paulson et al.[11] and Aschmann and Atkinson[12] both proposed that most •OH comes from the methyl vinyl carbonyl oxide (**7**), with a small contribution from formaldehyde oxide (**8**).

Later, Cremer and co-workers[10] reported extensive density functional theory (B3LYP) and MP2 studies on all the carbonyl oxides formed in isoprene ozonolysis, including all stable conformations of **7**. Their quantum chemical results (Scheme
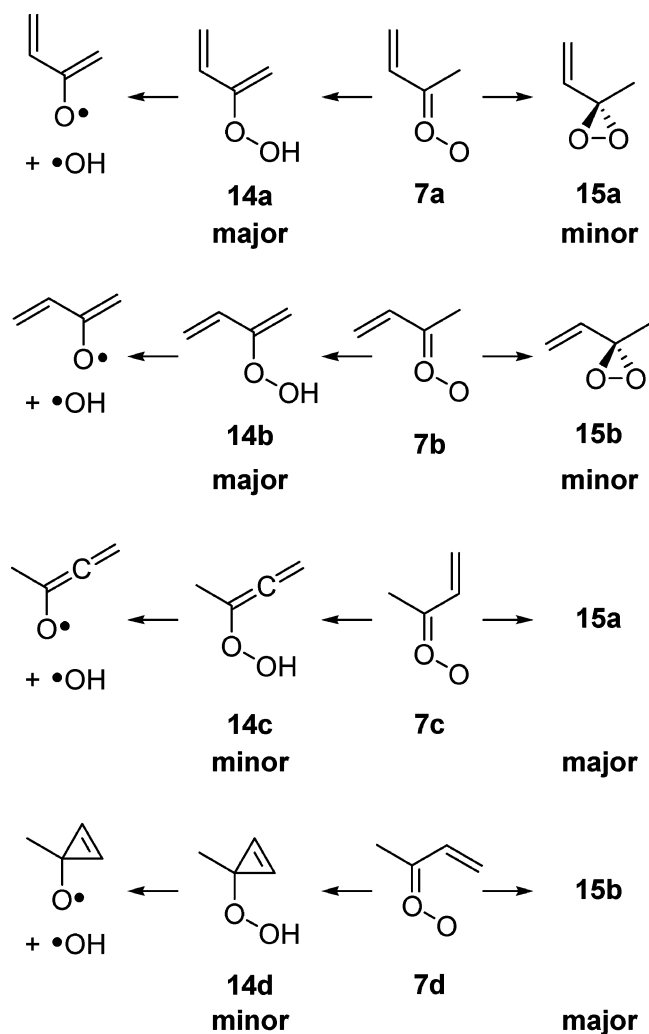
    * To whom correspondence should be addressed. E-mail: kuwata@macalester.edu.

SCHEME 1
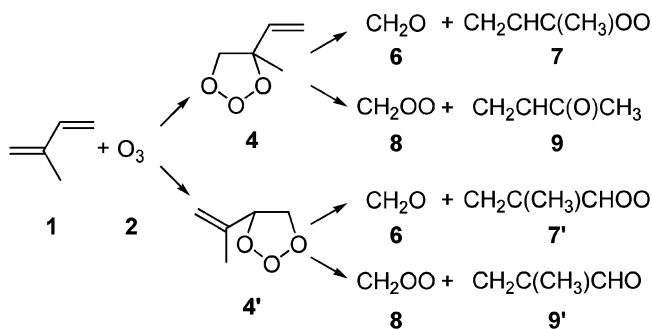
2) agreed with the previous proposals[11,12] that **7** will be the major source of •OH. More specifically, Cremer and co-workers predicted that the major isomerization product for conformers of **7** with the methyl group *syn* to the terminal oxygen (**7a** and **7b**) will be vinyl hydroperoxides **14a** and **14b**, formed by relatively facile 1,4-hydrogen shifts. Species **14a** and **14b** then decompose quantitatively to form •OH. In contrast, the major isomerization product of conformers of **7** with the vinyl group *syn* to the terminal oxygen (**7c** and **7d**) will be dioxiranes **15a** and **15b**.

More recently, Zhang and co-workers[13,14] reported a comprehensive theoretical study of the formation and cycloreversion of both **4** and **4'** (Scheme 1), as well as the unimolecular reactions previously considered by Cremer and co-workers for both **7** (Scheme 2) and **7'**. Their treatment combined quantum chemistry, employing a method approximating a CCSD(T)/6-311++G(d,p) calculation, and RRKM/master equation simulations to predict the branching ratios for both primary ozonide cycloreversion and carbonyl oxide isomerization. The cycloreversion channels forming **7** were predicted to be the most favorable, with a combined branching ratio of 0.47. The predicted rate constant for isoprene ozonolysis (1.58×10^{-17} cm^3 molecule^{-1} s^{-1}) and MVK yield (0.12) were in good

SCHEME 2

SCHEME 3

or dioxiranes (**15a** and **15b**) (Scheme 2). The ring closure we propose in this paper is analogous to reactions newly discovered by Vereecken and Peeters[29] for isoprene peroxy radicals (e.g., Scheme 4).

SCHEME 4

Second, we explore the effect of the vinyl group on the barriers to interconversion among the four conformers of **7** (Scheme 5). The fact that the C=C and C=O bonds of **7** are conjugated (as shown for conformer **7a** in Scheme 6) suggests that **TS10a−b** and **TS10c−d** will be somewhat higher in energy than transition structures for rotation about carbon−carbon single bonds. Recent calculations on isoprene carbonyl oxides by Aplincourt and Anglada bear this out.[30] By the same

SCHEME 5

SCHEME 6
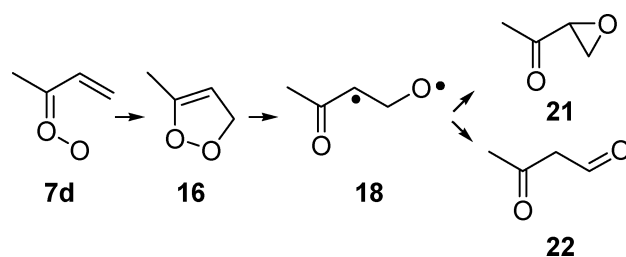

agreement with experiment.[3,12,15−23] Species **7**, the sole •OH precursor in their study, gave a predicted •OH yield of 0.25. This was in excellent agreement with some,[24−26] but not all,[6,21,27,28] experimental measurements. It is important to note that the majority of the •OH (0.14 of the 0.25) predicted by Zhang and co-workers comes from the 1,4-hydrogen shift in thermalized, not chemically activated, **7a** and **7b**.

While much is already understood about the mechanism of isoprene ozonolysis and its atmospheric impact, a good deal remains unexplored. The main goal of this paper will be to reexamine the chemistry of all four conformers of the methyl vinyl carbonyl oxide **7**, the most important isoprene ozonolysis intermediate. Our contention is that the vinyl group has a significant impact on the unimolecular reactivity of this species, an impact which has received little attention in the literature.
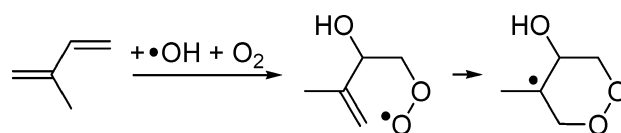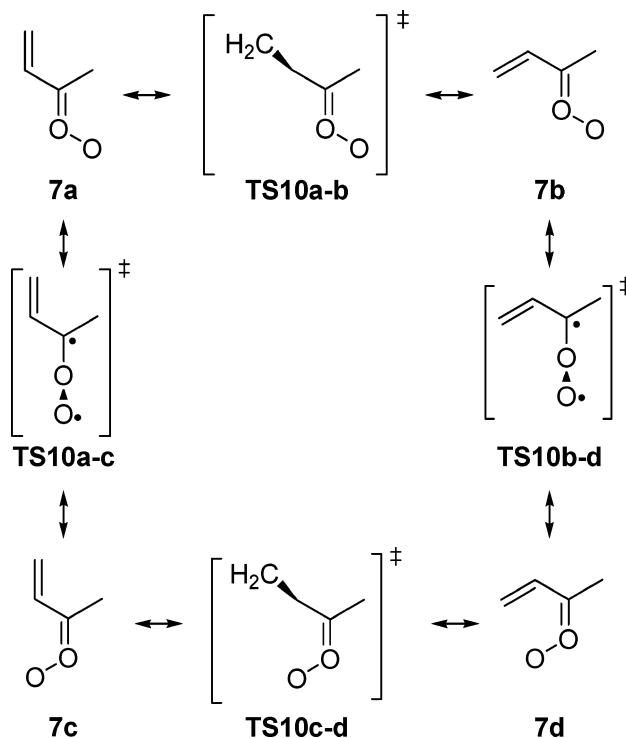
First, many of the carbon-containing products from isoprene ozonolysis have not been speciated, let alone quantified. We propose that a significant fraction of oxidized products arises from the electrocyclization and subsequent rearrangements of conformer **7d** (Scheme 3). The presence of a vinyl group synperiplanar to the O−O bond allows for a type of isomerization not available to carbonyl oxides derived from alkenes with only one double bond. We will present computational evidence that the yield of 5-methyl-3*H*-1,2-dioxole (**16**) from chemically activated methyl vinyl carbonyl oxide is higher than the yields of either vinyl hydroperoxides (**14a**, **14b**, and **14c**)

argument, **TS10a−c** and **TS10b−d** should be lower in energy than transition structures for rotation about carbon−oxygen double bonds. We are not aware of any study of this issue in the literature. In this paper, we provide detailed quantum chemical evidence for both contentions. Moreover, our RRKM/master equation simulation results indicate that the ability of chemically activated methyl vinyl carbonyl oxides to undergo rotation about their C=O bonds significantly enhances the dioxole branching ratio.

II. Theoretical Methods

A. Quantum Chemistry Calculations. All electronic structure calculations were performed with the Gaussian 03 suite of programs.[31] The geometry, energy, and harmonic vibrational frequencies of each stationary point considered here were determined initially using the B3LYP functional[32,33] and the 6-31G(d,p) basis set.[34,35] Each reported minimum has all real frequencies, and each reported transition structure has one imaginary frequency. We determined the minima associated with each transition structure by animation of the imaginary frequency and, if necessary, with intrinsic reaction coordinate (IRC) calculations.[36,37]

Because the B3LYP method tends to underestimate hydrogen-shift reaction barriers and can provide unreliable thermochemical predictions,[38−44] we further characterized each stationary point using the CBS-QB3 composite method of Petersson and co-workers.[45] This model chemistry, which employs B3LYP/6-311G(2d,d,p) optimized geometries and vibrational frequencies, uses a series of single-point calculations to extrapolate the CCSD(T) energy[46] to the complete basis set limit. (The Gaussian 03 implementation of CBS-QB3 correctly computes an empirical correction term based on overlap integrals, fixing a Gaussian 98 error noted by Green and co-workers.[47]) The singlet diradical species in this study (such as **TS10a−c** and **TS10b−d** in Scheme 5) were treated with wave functions of broken spin symmetry both for geometry optimizations (using unrestricted (U) B3LYP theory) and for the single-point energy calculations in the CBS-QB3 procedure (using UHF theory to compute the reference wave functions). All CBS-QB3 relative energies reported here are corrected for differences in zero-point vibrational energy scaled by 0.99.

To aid in the interpretation of our quantum chemical results, we performed natural bond order (NBO) analyses of the SCF density of selected structures using the NBO 5.0 program of Weinhold and co-workers.[48] NBO analysis was performed on the B3LYP/6-311G(2d,d,p) optimized geometries. We paid particular attention to natural population analysis (NPA) charges[49] and the Lewis structures and bond orders predicted by natural resonance theory (NRT).[50−52]

Recent studies indicate that CBS-QB3 often provides excellent agreement with experimental reaction energies and barriers, in some cases with greater accuracy than single-point CCSD(T) calculations with polarized triple-ζ basis sets.[53−57] It is possible, then, that our CBS-QB3 predictions will be more accurate than the CCSD(T)/6-31G(d)+CF//B3LYP/6-31G(d,p) method used by Zhang and co-workers to treat isoprene ozonolysis.[13,14,58,59] (The "CF," or correction factor, approximates the effect of expanding the basis set from 6-31G(d) to 6-311++G(d,p) at the CCSD(T) level.) Comparison of the predictions of the two methods will be made whenever possible.

However, Coote has recently reported[38] that CBS-QB3 systematically underestimates *inter*molecular hydrogen-transfer barriers in monoradicals by ~0.5 kcal/mol as compared to the very high level W1 method of Martin et al.,[60] perhaps because

CBS-QB3 overcompensates for the effects of spin contamination in *open*-shell species. The hydrogen-transfer reactions in our system are *intra*molecular shifts in (largely) *closed*-shell carbonyl oxides[9,61] and may therefore be expected to be accurate. Nevertheless, we will address the possibility that CBS-QB3 is underestimating hydrogen-shift barriers in our master equation modeling.

The B3LYP hybrid functional, like other generalized gradient approximation methods, does not treat dispersion forces explicitly.[62−64] Therefore, it often fails to predict the existence of van der Waals complexes[65,66] and severely underestimates the barriers of loose transition structures.[42] Experiment and ab initio calculations indicate that this is precisely the situation that exists in the first part of the ozonolysis reaction coordinate (Scheme 7).[67]

SCHEME 7

r(C-O): 3.24[a] 2.101[b] 1.417[a]
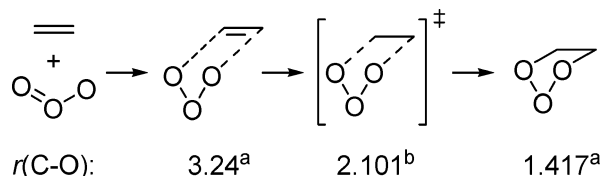
[a] Experimental value from Gillies et al.[68] [b]CASSCF(10,9)/cc-pVTZ value from Ljubic and Sabljic.[69]

Microwave spectroscopy[68] reveals that for the ethene−ozone system, the reactants form a van der Waals complex with C−O bonds of over 3.2 Å. At the cycloaddition transition state, the C−O bonds are predicted by CASSCF(10,9)/cc-pVTZ calculations[69] to be more than 2 Å long. Hence, it is not surprising that CBS-QB3, which is based on B3LYP geometries, has trouble predicting a physically reasonable value for the isoprene−ozone cycloaddition barrier. We attempted to correct for this deficiency by optimizing the cycloaddition transition structure geometry using the MPWB1K hybrid meta density functional of Zhao and Truhlar.[70] The MPWB1K method has been parametrized to treat noncovalent interactions and transition structure geometries accurately. MPWB1K calculations were performed using the MG3S basis set recommended by Truhlar and co-workers.[71]

B. Statistical Rate Theory Calculations. We used Barker's MultiWell program suite[72,73] to solve the one-dimensional (internal energy) master equation for both the cycloreversion of the primary ozonide and the isomerization of the methyl vinyl carbonyl oxides. The zero-point corrected relative energies of all participating species were taken from our CBS-QB3 calculations. Microcanonical rate constants $k(E)$ were computed using Rice−Ramsperger−Kassel−Marcus (RRKM) theory,[74] with the required sums and densities of states being calculated based on B3LYP/6-311G(2d,d,p) optimized geometries and unscaled harmonic frequencies. We did not treat low-frequency internal rotations as hindered rotors, a simplification that may affect the numerical accuracy of our results[75] but should not detract from the validity of our qualitative conclusions.[76]

We treated collisional stabilization with the exponential-down model, using an energy grain size of 10 cm^{-1} and assuming an average energy transferred per collision ($\langle E_d \rangle$) of 300 cm^{-1}.[77] The bath gas was N$_2$ at 298 K, with Lennard-Jones parameters of $\sigma = 3.74$ Å and $\epsilon = 82$ K.[78,79] Estimating the Lennard-Jones parameters for the isoprene ozonolysis intermediates involved the use of a number of different methods. First, we used the group contribution method of McCann and Danner[80] to determine an expression for each species' second virial coefficient as a function of temperature and the species' critical temperature

Methyl Vinyl Carbonyl Oxides

J. Phys. Chem. A, Vol. 109, No. 47, 2005 **10713**

TABLE 1: Zero-Point Corrected Relative Energies (kcal/mol) for the Species in Reactions 1 and 2

species	energy relative to species	CBS-QB3	CCSD(T)[a]
TS3	1 + 2	−1.2 (+1.8[b])	+3.3
4	1 + 2	−54.1	−48.1
TS5a	4	+12.3	+11.3
TS5b	4	+13.1	+11.9
TS5c	4	+13.3	+12.3
TS5d	4	+14.2	+13.1
TS5e	4	+15.0	
TS5f	4	+15.3	
TS5g	4	+15.4	+14.0
TS5h	4	+15.6	
6 + 7a	4	−9.1	−13.0
6 + 7b	4	−7.4	−11.6
6 + 7c	4	−6.2	−10.5
6 + 7d	4	−6.2	−10.3
8 + 9	4	−2.3	−7.1

[a] The CCSD(T)/6-31G(d)+CF//B3LYP/6-31G(d,p) results of Zhang and Zhang.[13] [b] Based on the MPWB1K/MG3S optimized geometry and vibrational frequencies scaled by 0.9567.[70]

(T_c). For the isoprene primary ozonides, we used Joback's approach[81,82] to estimate that $T_c = 620$ K. For the methyl vinyl carbonyl oxides, we assumed its T_c to be that of methyl acrylate, 536 K.[83] Then, following Hirschfelder's treatment,[84] we found the values of σ and ϵ consistent with the virial coefficient expressions we had derived. For the isoprene primary ozonides, $\sigma = 7.84$ Å and $\epsilon = 322$ K, and for the methyl vinyl carbonyl oxides, $\sigma = 6.29$ Å and $\epsilon = 358$ K.

Each simulation was run for 10^3 collisions to ensure that the pseudo steady state[85] was achieved. Trials were run at pressures of 1, 10, 50, 100, 200, 300, 400, 500, 600, and 760 torr. Typically, no more than 100 collisions (corresponding to ~50 ns at 760 torr) were required to converge the concentrations of all participating species to within the numerical noise of the simulation. Each pseudo-steady-state yield reported is the average of 10^5 simulations. In no case is the uncertainty in a yield greater than ±0.002. Details of how the initial energy distribution of a given species was represented in a given simulation are given in the Results and Discussion section below.

III. Results and Discussion

A. Primary Ozonide Formation and Decomposition: Structure and Energetics. Table 1 summarizes our CBS-QB3 and Zhang and Zhang's[13] CCSD(T) predictions for the energetics of the cycloaddition of ozone to isoprene (reaction 1) and the cycloreversion of the primary ozonide **4** (reactions 2a–h, Scheme 8). Figures 1 and 2 show the optimized structures for the species in reactions 1 and 2. (All structures were rendered using the Ball & Stick program of Müller and Falk.[86]) Note that we report only the most stable conformers of **1**, **TS3**, and **4** but report all eight possible conformers of **TS5**. Zhang and Zhang report only five conformers of **TS5**.

SCHEME 8[a]

[a] The boxed numbers above each arrow for reactions 2a–h are the 1-atm branching ratios for each channel predicted by our master equation simulations, as discussed in section IIIB.

TS3 to be 1.2 kcal/mol *below* that of the separated reactants **1** and **2**; CCSD(T)/6-31G(d)+CF predicts **TS3** to be 3.3 kcal/mol *above* **1** and **2**. Zhang and Zhang[13] corroborated the CCSD(T)/6-31G(d)+CF cycloaddition barriers (to both double bonds) by using transition state theory to predict rate constants for the addition of ozone to both the 1,2-double bond ($k_{12} = 0.93 \times 10^{-17}$ cm³ molecule⁻¹ s⁻¹ at 300 K) and the 3,4-double bond ($k_{34} = 0.65 \times 10^{-17}$ cm³ molecule⁻¹ s⁻¹ at 300 K). The sum of the two rate constants, 1.58×10^{-17} cm³ molecule⁻¹ s⁻¹, is close to recent experimental measurements ($k = (1.2-1.3) \times 10^{-17}$ cm³ molecule⁻¹ s⁻¹ at ~295 K).[15–18]

CBS-QB3 clearly fails to describe the ozone cycloaddition process adequately, probably due to the failure of B3LYP to predict a reasonable geometry for the transition structure. Cremer and co-workers have described the analogous failure of B3LYP in describing ethene ozonolysis.[87] (It is interesting that CCSD(T)/
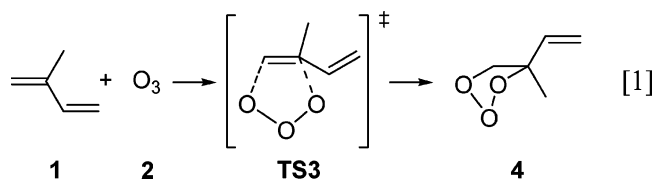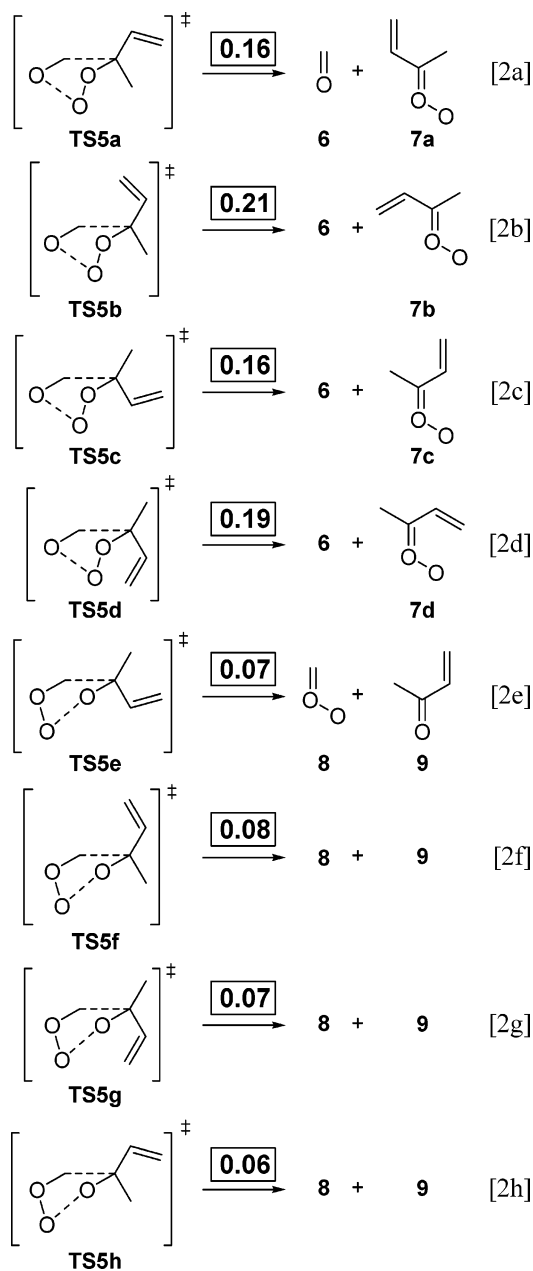
Table 1 reveals some significant differences between the two sets of energy predictions. The most obvious discrepancy regards the cycloaddition barrier. CBS-QB3 predicts transition structure
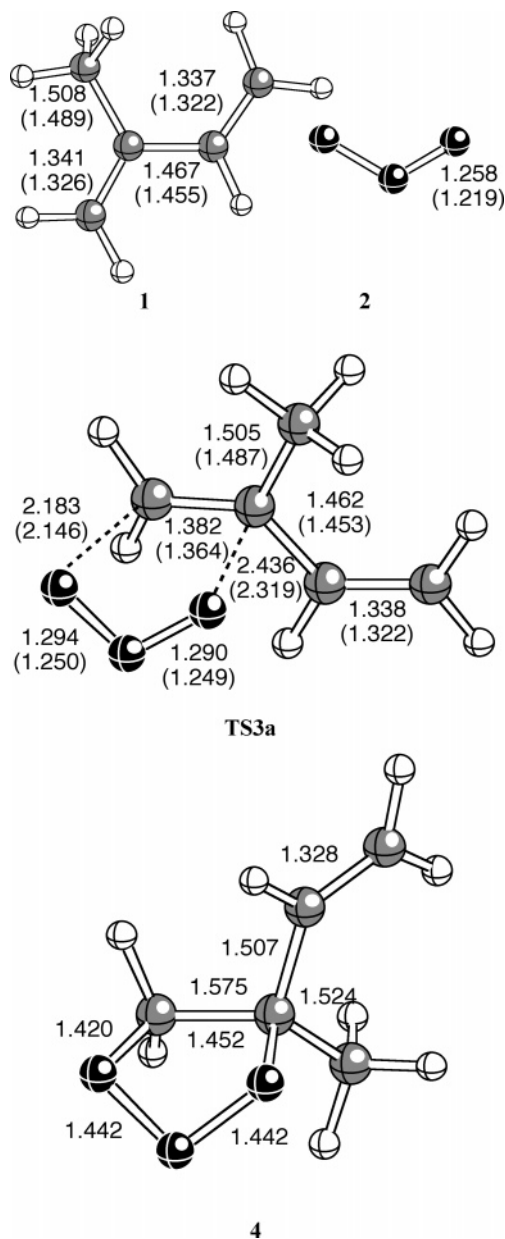
Figure 1. Optimized geometries for the species in reaction 1. Note that in this figure and in all others containing three-dimensional renderings of molecules, gray represents carbon, black represents oxygen, and white represents hydrogen. Bond lengths (in angstroms) obtained at the B3LYP/6-311G(2d,d,p) level; bond lengths (in angstroms) in parentheses obtained at the MPWB1K/MG3S level.

6-31G(d)+CF predicts a reasonable barrier despite the use of B3LYP/6-31G(d,p) geometries.) As discussed in section IIA, we reoptimized **TS3** with the MPWB1K/MG3S method. CBS-QB3 single-point calculations based on the MPWB1K geometry predict a cycloaddition barrier of 1.8 kcal/mol. While this is still 1.5 kcal/mol lower than the CCSD(T)/6-31G(d)+CF barrier, the CBS-QB3 barrier is now at least qualitatively reasonable.

Figure 1 shows the bond lengths predicted by the two density functional theory methods for **1**, **2**, and **TS3**. All of the MPWB1K bond lengths are shorter than the corresponding B3LYP bond lengths. In particular, all MPWB1K O−O bond lengths are ~0.04 Å shorter than those predicted by B3LYP. However, the B3LYP bond length in ozone, r(O−O) = 1.258 Å, is significantly closer to the experimental value[68] (1.276 Å) than the MPWB1K prediction.

There are other less dramatic, but still noteworthy, differences in the two sets of relative energy predictions in Table 1. First, our CBS-QB3 calculations predict that reaction 1 is ~6 kcal/mol more exothermic than the CCSD(T) calculations. The thermochemistry of primary ozonide formation remains a challenge for electronic structure theory. Even for the cyclo-addition of ozone to ethene, high-level theoretical estimates of reaction energy range from −49 to −54 kcal/mol (at 0 K).[88−90] Second, the cycloreversion barriers (**TS5**) predicted by the CCSD(T)/6-31G(d)+CF method are all ~1 kcal/mol lower than the CBS-QB3 barriers. In addition, the only transition structure (**TS5g**) leading to formaldehyde oxide (**8**) and MVK (**9**) reported by Zhang and Zhang is not the lowest energy barrier according to CBS-QB3. For this part of the reaction coordinate, there are no experimental data to adjudicate between the two sets of predictions.[91]

The two quantum chemical methods agree that the formation of **8** and **9** (reactions 2e−h) is 3−7 kcal/mol less exothermic than the formation of formaldehyde **6** and methyl vinyl carbonyl oxide **7** (reactions 2a−d). This thermochemistry can be rationalized in terms of the isodesmic reactions in Scheme 9.

Substitution of **6** by a methyl group and a vinyl group (reaction 3) stabilizes the carbonyl group substantially: the CBS-QB3 energy of reaction 1 is −24.4 kcal/mol. Wiberg et al.[92] have attributed this stabilization to the donation of electron density from the methyl and vinyl substituents to the electron deficient carbonyl carbon. However, the methyl and vinyl groups stabilize **8** even more: the CBS-QB3 energy of reaction 2 is −31.2 kcal/mol. We will consider the origin of the enhanced stability of **8**, as well as the relative stabilities of the four conformers of **7**, in section IIIC.

With respect to cycloreversion (reaction 2), both quantum chemical methods predict a correlation of reaction barrier with reaction energy. The transition structures which lead to products **8** and **9** are all 1−3 kcal/mol higher in energy than the transition structures which lead to the more stable products **6** and **7**. Moreover, Figure 2 shows that **TS5e−h** are all later structurally than **TS5a−d**, with breaking O−O bonds 0.03−0.06 Å longer and breaking C−C bonds 0.03−0.04 Å longer (except for **TS5c**).

B. Master Equation Simulations of Primary Ozonide Decomposition. We solved the master equation for the 1,2-primary ozonide **4** in order to quantify the competition between collisional stabilization of **4** and its decomposition via the eight cycloreversion transition states shown in Scheme 8. The initial energy of **4** was represented by a shifted thermal distribution[74] truncated at the energy of transition structure **TS3**.

The 1-atm pseudo-steady-state yields for each of the eight exit channels are presented in boxes in Scheme 8. Variation of yield with pressure is negligible to two significant figures. At pressures up to 1 atm, none of the highly chemically activated primary ozonide is collisionally stabilized. This agrees with previous predictions of primary ozonide behavior by Donahue and co-workers,[99] Zhang and co-workers,[13,14] Kroll et al.,[94] and Cremer and co-workers.[87]

Table 2 summarizes the cycloreversion branching ratios based on the type of carbonyl oxide formed, with **TS5a** and **TS5b** leading to carbonyl oxides with the methyl group syn to the O−O bond (**7a** and **7b**), **TS5c** and **TS5d** leading to carbonyl oxides with the vinyl group syn to the O−O bond (**7c** and **7d**), and **TS5e**, **TS5f**, **TS5g**, and **TS5h** leading to the parent carbonyl oxide (**8**) and MVK (**9**). Simulation results by Zhang and co-workers[14] are also tabulated for comparison.

Methyl Vinyl Carbonyl Oxides

J. Phys. Chem. A, Vol. 109, No. 47, 2005 **10715**
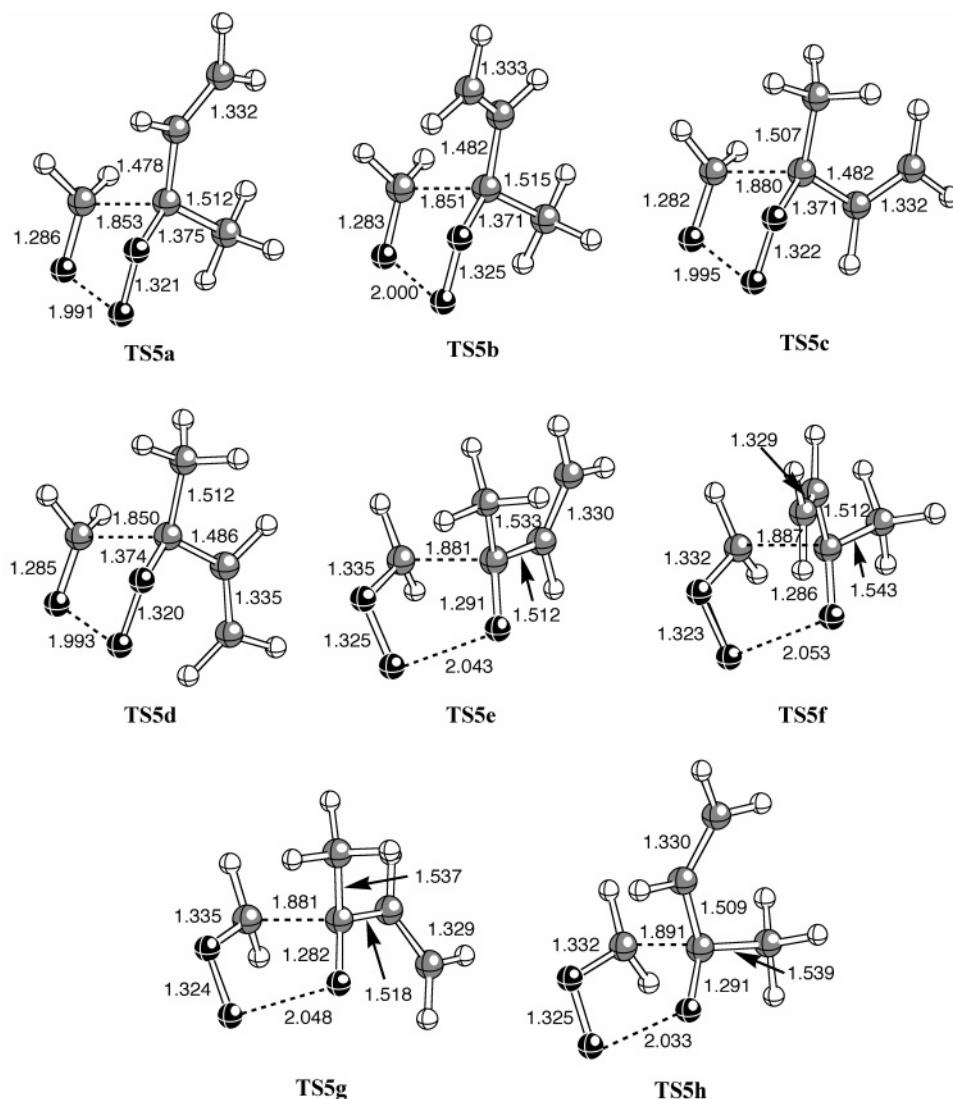
Figure 2. Optimized geometries for the transition structures in Scheme 8. Bond lengths (in angstroms) obtained at the B3LYP/6-311G(2d,d,p) level.

SCHEME 9
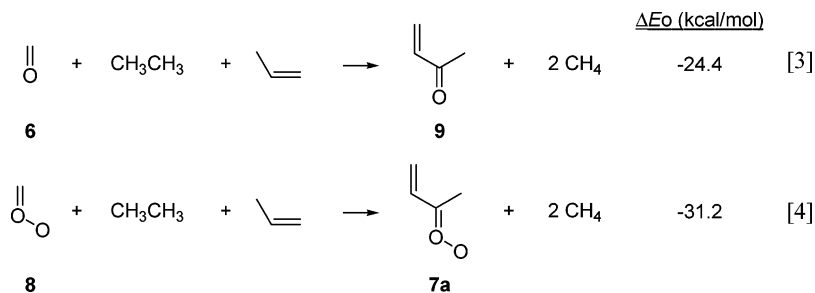
TABLE 2: Predicted Yields of Carbonyl Oxides Formed by Cycloreversion of the 1,2-Primary Ozonide

type of carbonyl oxide	this work	Zhang[a]
syn-methyl (7a and 7b)	0.37	0.44
syn-vinyl (7c and 7d)	0.35	0.35
parent (8)	0.28	0.21

[a] From Zhang and co-workers.[14]

We predict a significantly lower yield of **7a** and **7b** (and H$_2$CO), and a significantly higher yield of **8** (and MVK), than do Zhang and co-workers.[14] Much of this discrepancy is due to the fact that our simulation included all eight possible cyclo-

reversion transition structures, while Zhang and co-workers considered only the lowest energy channel leading to each type of carbonyl oxide. Higher energy transition structures, which will have a negligible impact on the reactivity of the thermalized primary ozonide, play a greater role in the reactivity of the chemically activated primary ozonide, since all of the ozonide is formed with energy in excess of the cycloreversion barriers.

One indirect confirmation of the validity of our simulation concerns the experimental yield of MVK. As mentioned in section IIIA, Zhang and Zhang[13] successfully used transition state theory to predict the initial rate of isoprene ozonolysis.
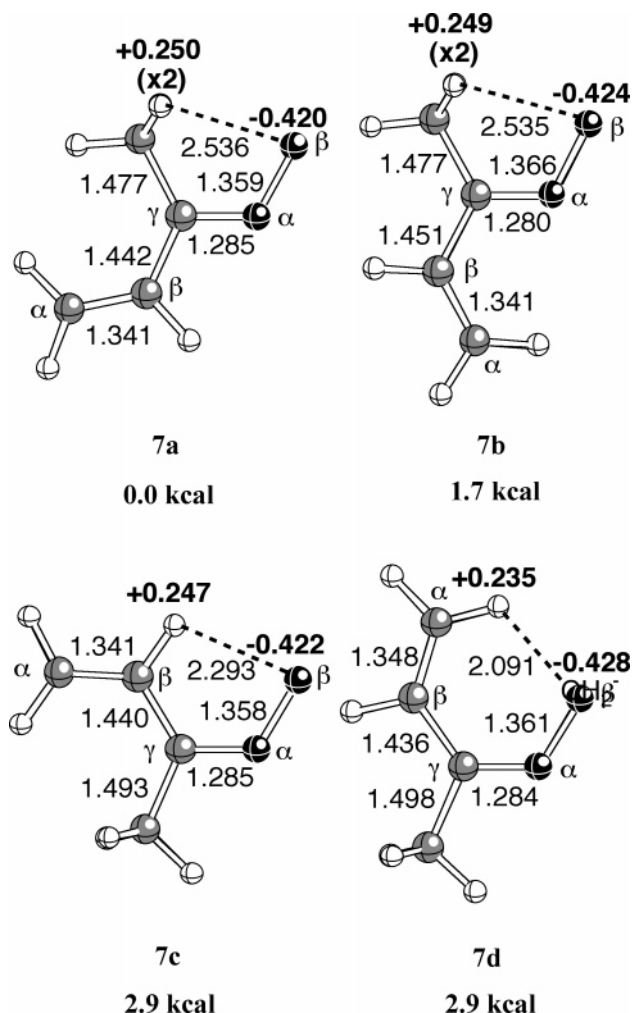
Figure 3. Optimized geometries for the four possible methyl vinyl carbonyl oxide conformers. Bond lengths (in angstroms) obtained at the B3LYP/6-311G(2d,d,p) level are shown in normal type; selected NPA charges are shown in boldface; 0 K relative energies (in kcal/mol) are from CBS-QB3 calculations.

Part of their prediction included an estimate of the branching ratio for ozone addition to the 1,2-double bond: $k_{12}/(k_{12} + k_{34})$ = 0.59. Weighing the yield (0.28) of **9** from the 1,2-primary ozonide **4** by the yield of **4** (0.59) gives an overall MVK yield of 0.17. This is in excellent agreement with the currently recommended experimental MVK yield of 0.159 ± 0.013.[3,12,23]

C. Structure and Interconversion of the Methyl Vinyl Carbonyl Oxides. Figure 3 shows the optimized geometries, relative energies, and selected NPA charges for the four methyl vinyl carbonyl oxides **7a**, **7b**, **7c**, and **7d**.

The CBS-QB3 relative stabilities of the four conformers are in good agreement with the CCSD(T)/6-31G(d)+CF predictions of Zhang and Zhang[13] and the G2M-RCC5//B3LYP predictions of Aplincourt and Anglada,[30] and in fair agreement with the B3LYP/6-31G(d,p) predictions of Cremer and co-workers.[10] As previously discussed by Cremer,[10,95] the conformers with a methyl group syn to the $O_\alpha-O_\beta$ bond will be preferentially stabilized by interactions between the methyl hydrogens and the terminal oxygen O_β. The NPA charges shown in Figure 3 support this contention; O_β and the methyl and vinyl hydrogens have roughly the same magnitude of charge in all four conformers. Therefore, **7a** and **7b**, which each have two attractive H- - -O_β interactions, are expected to be more stable than **7c** and **7d**.
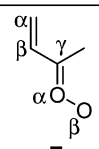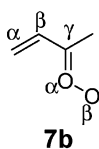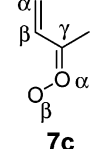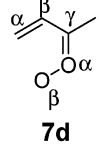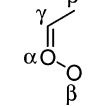
Among the two *syn*-methyl conformers, **7b** is predicted to be 1.7 kcal/mol less stable than **7a**. We can attribute **7b**'s lower stability to its synperiplanar $C_\alpha=C_\beta$ and $C_\gamma=O_\alpha$ bonds, which impart an unfavorable cyclic four-electron antiaromatic character, as previously discussed by Cremer and co-workers[10] and Houk and co-workers.[96] Like **7b**, conformer **7d** is also desta-bilized by an antiaromatic arrangement of its $C_\alpha=C_\beta$ and $C_\gamma=O_\alpha$ bonds. Based on the relative energies of **7a** and **7b**, we would expect this antiaromaticity would make **7d** ~2 kcal/mol less stable than **7c**. However, **7d** also has a positively charged vinyl hydrogen only 2.09 Å away from the negatively charged O_β. The corresponding hydrogen in **7c** is 2.29 Å away. The CBS-QB3 method predicts the destabilizing antiaromatic and the stabilizing electrostatic effects in **7d** to be roughly equal in magnitude, making **7c** and **7d** equal in stability (to two significant figures).

Scheme 10 shows the four most important resonance con-tributors to the electronic structure of the four conformers of **7**, with the percentage contribution of each Lewis structure calculated by NRT. For each conformer, the best Lewis structure contributes only ~50% to the overall electronic character. The second most important contributor has the connectivity, but not the geometry, of a dioxirane. (Note that the B3LYP calculations on which the NRT decomposition is based predict that **7** has no open-shell character. Other electronic structure methods, such as Goddard's GVB theory, would likely predict the singlet diradical, instead of the dioxirane, to be a major contributor.[93]) Both the third and the fourth best contributors will lower the barrier to rotation about the carbon—oxygen bond. In addition, the vinyl group in the fourth best contributor "pushes" electron density to the internal oxygen, eliminating the unfavorable positive formal charge present in the best and third best Lewis structures. This helps explain why a vinyl group would stabilize
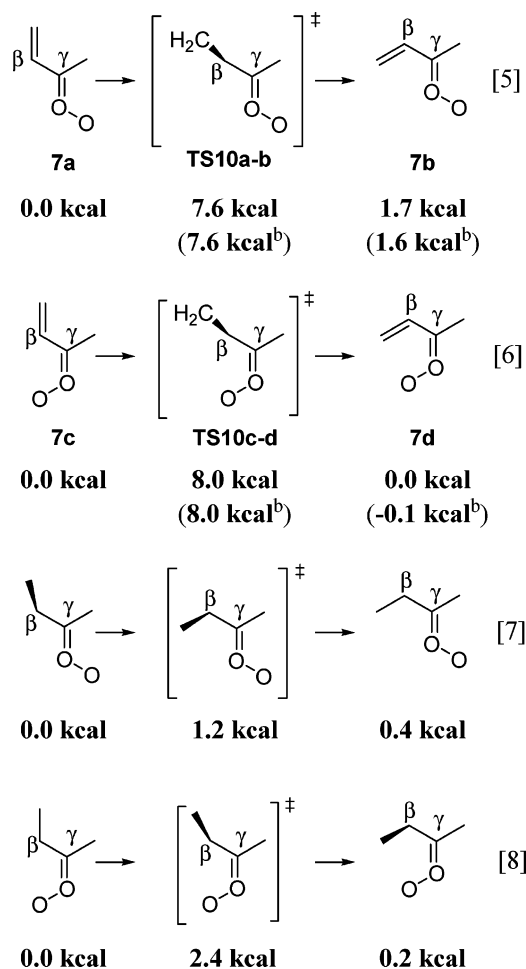
SCHEME 10

Methyl Vinyl Carbonyl Oxides

J. Phys. Chem. A, Vol. 109, No. 47, 2005 **10717**
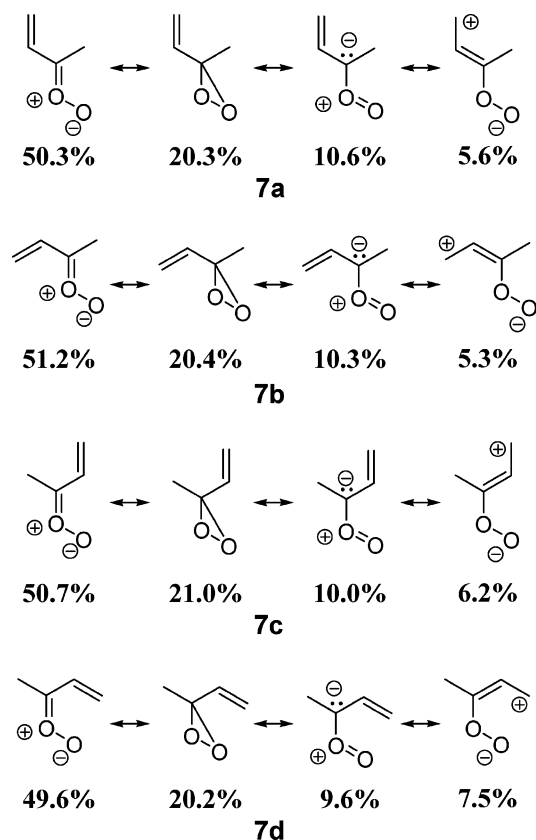
TABLE 3: Selected NRT Bond Orders for Various Carbonyl Oxides

structure	NRT bond order			
	C_α-C_β	C_β-C_γ	C_γ-O_α	O_α-O_β
7a	1.91	1.07	1.55	1.10
7b	1.93	1.06	1.56	1.10
7c	1.92	1.01	1.56	1.09
7d	1.90	1.09	1.56	1.08
	1.03	1.63		1.08

SCHEME 11[a]

[5]

7a — 0.0 kcal
TS10a-b — 7.6 kcal (7.6 kcal[b])
7b — 1.7 kcal (1.6 kcal[b])

[6]

7c — 0.0 kcal
TS10c-d — 8.0 kcal (8.0 kcal[b])
7d — 0.0 kcal (-0.1 kcal[b])

[7]

0.0 kcal — 1.2 kcal — 0.4 kcal
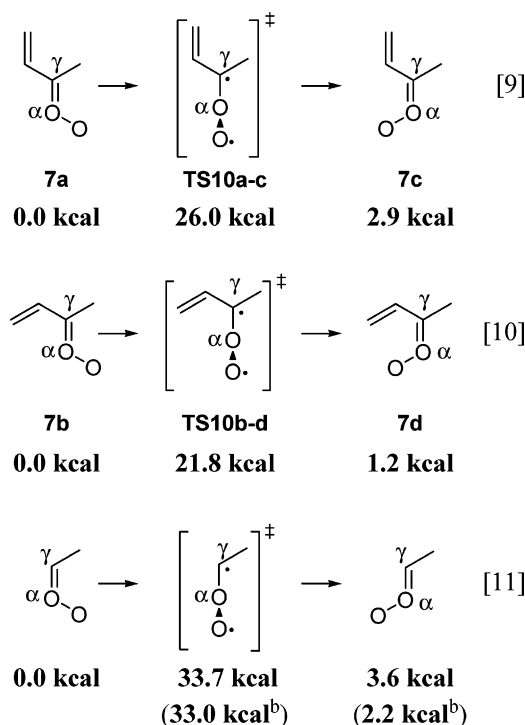
[8]

0.0 kcal — 2.4 kcal — 0.2 kcal

[a] The energy of each transition structure and product is relative to the energy of each reactant. [b] Relative energies in parentheses are from the G2M-RCC5//B3LYP calculations of Aplincourt and Anglada.[30]

a carbonyl oxide more than a carbonyl, as shown by the pair of isodesmic reactions in Scheme 9.

The overall effect of multiple nonnegligible resonance contributors on electronic structure can be quantified by the bond orders within the carbonyl oxide. Table 3 shows selected NRT bond orders predicted for all four conformers of **7**, as well as for *syn* acetaldehyde oxide. We see that in all cases, the C_β–C_γ and the O_α–O_β bonds have a slight amount of π-character, the C_α–C_β bond is slightly weaker than a full double bond and the C_γ–O_α bond is substantially weaker than a full double bond. Much of the decrease in the C_γ–O_α bond order is due to a substantial contribution from the dioxirane-like Lewis structure, as seen in Scheme 10. For this reason, *syn* acetaldehyde oxide, which lacks a double bond conjugated with its C_γ=O_α bond, has only a slightly higher C_γ–O_α bond order than the methyl vinyl carbonyl oxides. The vinyl group has a clear, but not large, effect on the C_γ–O_α bond order in **7**.

Finally, Schemes 11 and 12 report the CBS-QB3 barriers to rotation about the C_β–C_γ and the C_γ–O_α bonds of various carbonyl oxides, and Figure 4 shows the optimized geometries for the methyl vinyl carbonyl oxide rotation transition structures. The barriers to rotation about the C_β–C_γ single bond in 2-butanone oxide (reactions 7 and 8), which are 1−2 kcal/mol, are 5−7 kcal/mol lower than the C_β–C_γ rotation barriers in methyl vinyl carbonyl oxide (reactions 5 and 6). The energetics for reactions 5 and 6 are in excellent agreement with the G2M-RCC5//B3LYP calculations of Aplincourt and Anglada.[30] The difference in barriers reflects the small, but not negligible,

amount of π-character in **7**'s C_β–C_γ bond, as evidenced in the NRT bond orders (Table 3). Also note that the C_β–C_γ bond lengths in **TS10a**−**b** and in **TS10c**−**d** (Figure 4) are 0.02−0.05 Å longer than the corresponding bonds in **7a**−**d** (Figure 3). This is consistent with the idea that the C_β–C_γ bond in **7** possesses π-character which is lost at the rotation transition state.

CBS-QB3 predicts that the barriers to rotation about the C_γ=O_α bond in the methyl vinyl carbonyl oxides (reactions 9 and 10) are 8−12 kcal/mol lower than the analogous barrier to rotation in acetaldehyde oxide (reaction 11). The energetics for reaction 11 are in good agreement with the MRDCI+Q// CASSCF predictions of Anglada et al.[9] A simple argument based on resonance structures would predict that **TS10a**−**c** and **TS10b**−**d** should be lower in energy than the rotation transition state in reaction 11 based on the ability of the vinyl group to delocalize the unpaired electron on C_γ (Scheme 13).

Support for this argument comes from the B3LYP/6-311G(2d,d,p) geometries. In **TS10a**−**c** and **TS10b**−**d** (Figure 4), the C_α=C_β bonds are 0.03−0.04 Å longer and the C_β=C_γ bonds are 0.05−0.08 Å shorter than the corresponding bonds in **7a**−**d** (Figure 3). We do not have a qualitative explanation for why reaction 10's barrier is ~4 kcal/mol lower in energy than reaction 9's barrier. However, the fact that the barrier to rotation in reaction 10 is comparable to the hydrogen-shift and dioxirane-closure barriers (as presented in section IIID) means that the common assumption[9,13,14,94,97−99] that rotation about

SCHEME 12[a]

[9]

7a   **TS10a-c**   **7c**

0.0 kcal   **26.0 kcal**   **2.9 kcal**

[10]

7b   **TS10b-d**   **7d**

0.0 kcal   **21.8 kcal**   **1.2 kcal**

[11]

0.0 kcal   **33.7 kcal**   **3.6 kcal**

                   (33.0 kcal[b]**)**   **(2.2 kcal**[b]**)**
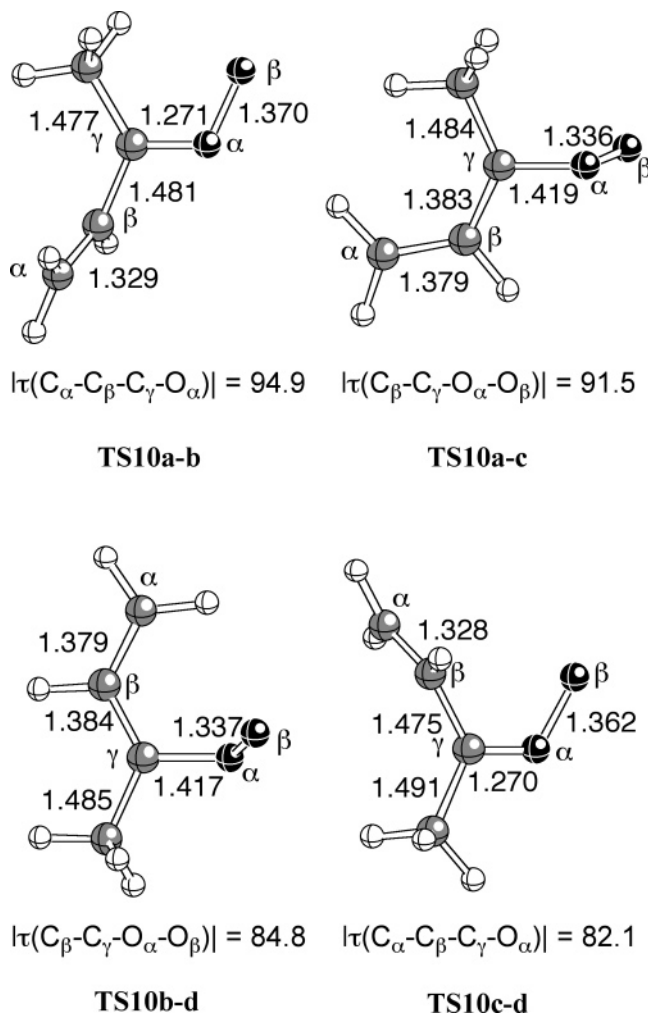
[a] The energy of each transition structure and product is relative to the energy of each reactant. [b]Relative energies in parentheses are from the MRDCI+Q//CASSCF calculations of Anglada et al.[9]

C=O bonds in carbonyl oxides is negligible is not justified for the isoprene system.

D. Other Unimolecular Reactions of the Methyl Vinyl Carbonyl Oxides. Scheme 14 shows the other possible isomerization reactions of the methyl vinyl carbonyl oxides **7a–d**, and Table 4 summarizes both the CBS-QB3 and the CCSD(T)/6-31G(d)+CF[13] predictions of the relative energies of each minimum and transition structure in this scheme. Figure 5 shows the optimized structures for the species involved in reactions 18 and 19.

As noted previously by Cremer and co-workers[10] and Zhang and Zhang,[13] the 1,4-shift of a methyl hydrogen is somewhat more favorable than the 1,4-shift of a vinyl hydrogen, with the CBS-QB3 barriers for reactions 12 and 14 being 3–4 kcal/mol lower than the barrier for reaction 16. With regard to dioxirane formation (reactions 13, 15, 17, and 19), Cremer et al.[100] observed that for the parent carbonyl oxide, ring closure is initiated by pyramidization at the carbon atom. This paradigm also applies to the methyl vinyl carbonyl oxides under consideration here. For example, in **TS12d** (Figure 5) the torsional angles about the C_γ–O_α bond are −66.1° and 125.0°, as compared to exactly 0° and 180° in reactant **7d**. In addition, **TS12d** is 3–5 kcal/mol higher in energy than the other dioxirane transition structures due to steric interactions between O_β and the vinyl group.

In **7d**, the relative orientation of the carbonyl oxide and vinyl groups allow for another ring-closing pathway, reaction 18, which forms 5-methyl-3H-1,2-dioxole (**16**). As mentioned in the Introduction, dioxole formation has not previously been considered in isoprene ozonolysis. This reaction can be classified as a 1,5-electrocyclization or, equivalently (following Huisgen[101]), as the intramolecular cycloaddition of the carbonyl oxide 1,3-dipole to the alkene. The geometry of the cyclization transition structure **TS13** (Figure 5) has the hallmarks[102,103] of a monorotatory pericyclic process. These include significant

$|\tau(C_\alpha\text{-}C_\beta\text{-}C_\gamma\text{-}O_\alpha)| = 94.9$ $|\tau(C_\beta\text{-}C_\gamma\text{-}O_\alpha\text{-}O_\beta)| = 91.5$

TS10a-b   **TS10a-c**

$|\tau(C_\beta\text{-}C_\gamma\text{-}O_\alpha\text{-}O_\beta)| = 84.8$ $|\tau(C_\alpha\text{-}C_\beta\text{-}C_\gamma\text{-}O_\alpha)| = 82.1$

TS10b-d   **TS10c-d**

Figure 4. Optimized geometries for the methyl vinyl carbonyl oxide rotation transition structures. Bond lengths (in angstroms) and torsional angles (in degrees) obtained at the B3LYP/6-311G(2d,d,p) level.
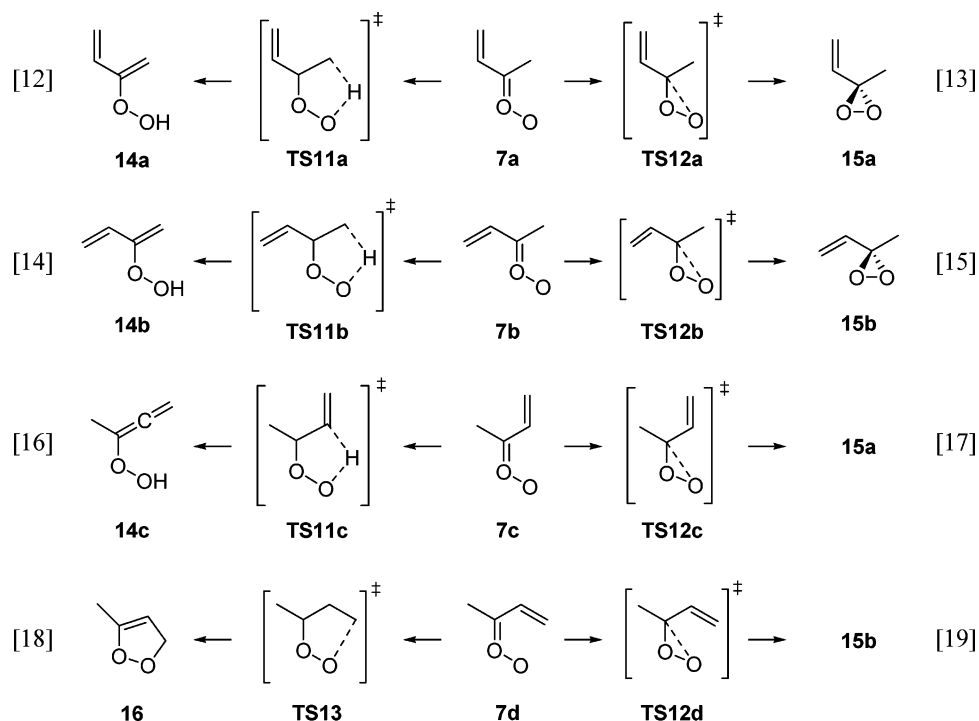
SCHEME 13

TS10a-c   **TS10b-d**
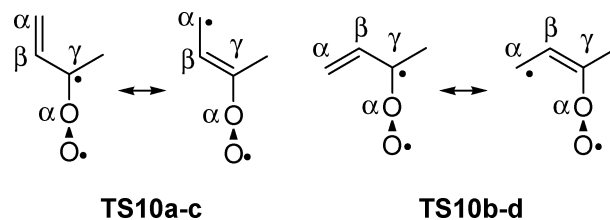
rotation of the vinyl group out of the plane of the carbonyl oxide moiety (the torsional angles about the C_α–C_β bond are +61.2° and −141.9°), significant lengthening of the double bonds (compared to the geometry of **7d**, $r(C_\alpha$–$C_\beta)$ increases by 0.05 Å and $r(C_\gamma$–$O_\alpha)$ increases by 0.03 Å), and significant shortening of the single bond ($r(C_\beta$–$C_\gamma)$ decreases by 0.05 Å).

Cyclization of vinyl carbonyl oxides to form dioxoles has some precedence in the organic literature.[104–106] Scarpati and co-workers, who have studied the rearrangements of furan endoperoxides such as **A** in deuteriochloroform, have obtained indirect evidence for carbonyl oxide **B** and NMR spectra of dioxole **C** (Scheme 15).[104]

Finally, Table 4 shows that the CBS-QB3 and CCSD(T)/6-31G(d)+CF methods predict relative stabilities for the carbonyl oxides (as noted in section IIIC) and their isomerization products **14** and **15** that agree to within 1 kcal/mol. The predicted barriers against dioxirane formation (**TS12**) agree almost exactly. In

Methyl Vinyl Carbonyl Oxides

J. Phys. Chem. A, Vol. 109, No. 47, 2005 **10719**

SCHEME 14

TABLE 4: Zero-Point Corrected Energies (kcal/mol, Relative to 7a) for Scheme 14

species	CBS-QB3	CCSD(T)[a]	species	CBS-QB3	CCSD(T)[a]
7a	0.0	0.0	TS12c	19.7	20.0
7b	1.7	1.5	TS12d	24.9	24.9
7c	2.9	2.5	TS13	13.9	
7d	2.9	2.7	14a	−12.9	−13.7
TS11a	18.0	18.8	14b	−14.7	−14.9
TS11b	19.1	19.9	14c	−0.1	−0.8
TS11c	21.7	24.4	15a	−18.6	−18.2
TS12a	22.2	22.1	15b	−17.1	−17.0
TS12b	20.9	21.0	16	−25.6	

[a] The CCSD(T)/6-31G(d)+CF//B3LYP/6-31G(d,p) results of Zhang and Zhang.[13]

SCHEME 15
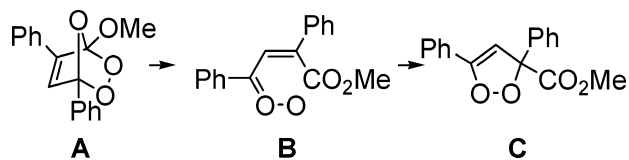
contrast, the CBS-QB3 hydrogen-shift barriers (**TS11**) are all 1−2 kcal/mol lower than the CCSD(T)/6-31G(d)+CF barriers. As discussed in section IIA, we are not aware of any evidence that CBS-QB3 systematically underestimates the barriers of intramolecular hydrogen transfers in closed-shell molecules such as carbonyl oxides. Nevertheless, we will address the possibility of underestimated hydrogen-shift barriers in the next section.

E. Master Equation Simulations of Carbonyl Oxide Chemistry. As discussed in section IIIB, 28% of the 1,2-primary ozonide **4** forms formaldehyde oxide (**8**) and MVK (**9**), while 72% of **4** forms formaldehyde (**6**) and substituted carbonyl oxide (**7**) (Scheme 8 and Table 2). Species **8** is formed vibrationally excited and will undoubtedly undergo further unimolecular reaction. We did not perform master equation simulations on **8**, but we will discuss its chemistry briefly in section IIIF.

We did perform master equation calculations on the chemically activated methyl vinyl carbonyl oxides, predicting their

fates as a function of pressure. The simulations included rotation about the C_β−C_γ bond (reactions 5 and 6, Scheme 11), rotation about the C_γ=O_α bond (reactions 9 and 10, Scheme 12), and formation of hydroperoxides, dioxiranes, and dioxoles (reactions 12−19, Scheme 14). For each simulation, the formation of one of the four carbonyl oxides **7x** (where **x** = **a**, **b**, **c**, or **d**) was the entrance channel. The initial energy distribution of each chemically activated carbonyl oxide was modeled as shown in Scheme 16.

Following Forst's treatment,[107] we assumed that the energy difference $E^\dagger$ between the ozone cycloaddition transition structure (**TS3**) and each of the primary ozonide cycloreversion transition structures (**TS5x**) goes into the internal degrees of freedom of the corresponding carbonyl oxide **7x** and the co-generated formaldehyde **6**, while E_o goes into the translation of **6** and **7x**. In turn, the energy $E^\dagger$ is partitioned between species **6** and **7x** as described by eq 20

$$f^{7x}(E) = \frac{\rho_{7x}(E)W_6(E^+ - E)}{\int_0^{E^+} \rho_{7x}(\epsilon)W_6(E^+ - \epsilon)\,d\epsilon} \tag{20}$$

where $f^{7x}(E)$ is the fraction of carbonyl oxide **7x** possessing energy E, ρ_{7x} is the density of states of **7x**, and W_6 is the sum of states of **6**. This approach to modeling the initial energy distributions of carbonyl oxides formed in ozonolysis has also been taken by Zhang and co-workers,[14] Kroll et al.,[94] and Cremer and co-workers.[87]

The possible exit channels in each simulation were vinyl hydroperoxide (**14a**, **14b**, or **14c**), dioxirane (**15a** or **15b**), or dioxole (**16**) (Scheme 14). Formation of any of these products was assumed to be irreversible, which is reasonable given their subsequent chemistry (see section IIIF). The other four possible outcomes of the simulation were collisional stabilization into one of the carbonyl oxide (**7a**, **7b**, **7c**, or **7d**) "wells." The overall yield for each exit channel or well was the sum of yields from each of the four simulations weighted by the branching ratio (Scheme 8) for the cycloreversion transition structure producing
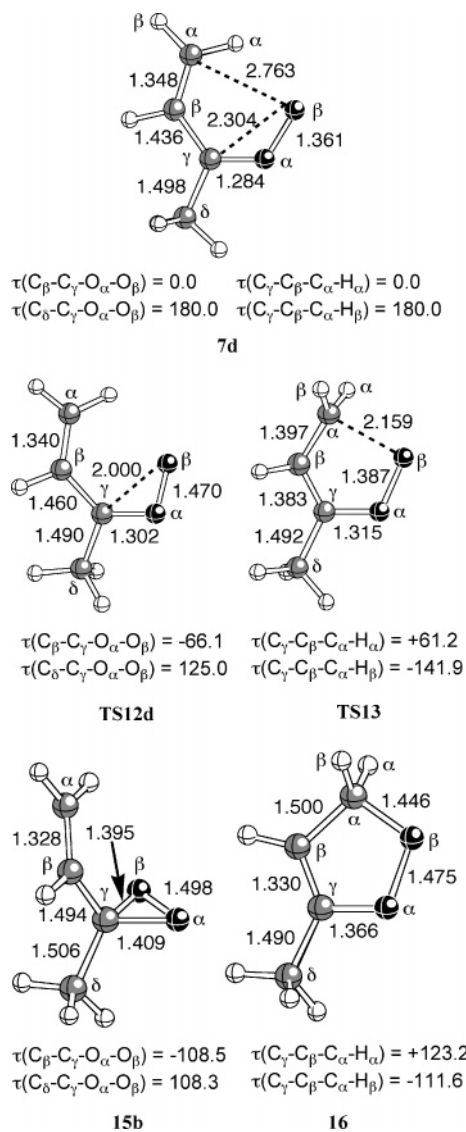
Figure 5. Optimized geometries for the structures in reactions 18 and 19. Bond lengths (in angstroms) and torsional angles (in degrees) obtained at the B3LYP/6-311G(2d,d,p) level.

SCHEME 16
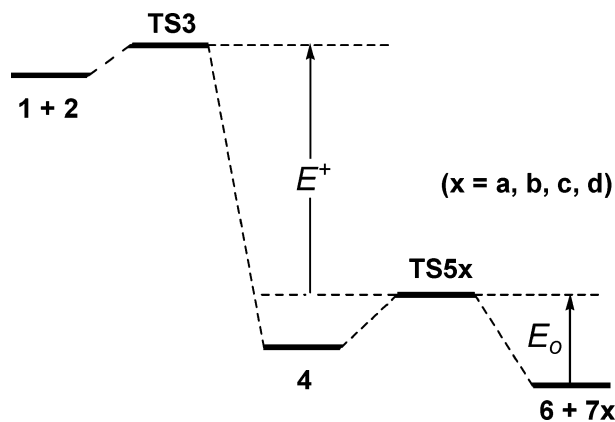
that simulation's entrance channel. The overall yields for the 12 exit channels and wells were then normalized to add up to 1.00.

Table 5 reports the pseudo-steady-state yields at 1 atm for each of the exit channels and wells and for the four categories of products under a variety of simulation conditions. Case 1 refers to the set of simulations performed as described above.

TABLE 5: 1-atm Yields from Methyl Vinyl Carbonyl Oxide Chemistry under Various Conditions

| exit channel or well	case 1[a]	case 2[b]	case 3[c]	case 4[d]	Zhang[e]
7a	0.14	0.06	0.13	0.19	
7b	0.01	0.12	0.01	0.02	
7c	0.02	0.10	0.01	0.01	
7d	0.01	0.01	0.01	0.02	
all carbonyl oxides	0.18	0.29	0.16	0.24	0.56
14a (from 7a)	0.24	0.15	0.22	0.18	
14b (from 7b)	0.07	0.12	0.04	0.05	
14c (from 7c)	0.01	0.04	0.01	0.01	
all hydroperoxides	0.32	0.31	0.27	0.24	0.19
15a (from 7a)	0.03	0.02	0.13	0.03	
15b (from 7b)	0.02	0.05	0.05	0.04	
15a (from 7c)	0.03	0.08	0.02	0.03	
15b (from 7d)	0.00	0.00	0.01	0.00	
all dioxiranes	0.08	0.15	0.21	0.10	0.26
dioxole (16)	0.42	0.25	0.36	0.42	0.00

[a] Includes all possible isomerization reactions. [b] All interconversions among carbonyl oxides conformers (reactions 5, 6, 9, and 10) are neglected. [c] All rotations about C=O bonds (reactions 9 and 10) are neglected. [d] All CBS-QB3 hydrogen shift barriers (**TS11a**, **TS11b**, and **TS11c**) raised by 1 kcal/mol. [e] From Zhang and co-workers.[14]

These calculations predict that the most important pathway for the methyl vinyl carbonyl oxide is dioxole formation, with a yield of 0.42. Vinyl hydroperoxide formation is also important, with a total yield of 0.32. Dioxirane formation is far less important, with a total yield of 0.08. The remaining 18% of the carbonyl oxide is predicted to be collisionally stabilized and not undergo unimolecular reaction, at least on a "prompt" time scale.

Examining case 1 results in more detail, we see that the contributions made by **7a−c** to the hydroperoxide yield decreases in order of increasing hydrogen-shift reaction barrier (**TS11a**, **TS11b**, and **TS11c**, Table 4), as expected. Interestingly, **7a**, which makes the largest contribution (0.24) to the overall hydroperoxide yield also makes the largest contribution (0.14) to the overall stabilized carbonyl oxide yield, since **7a** is the lowest energy conformer. The relative unimportance of the dioxirane channels is due largely to the difference in reaction barriers; the lowest energy dioxirane transition structure, **TS12c**, is ~2 kcal/mol less stable than the lowest energy hydrogen-shift transition structure (**TS11a**) and ~6 kcal/mol less stable than the dioxole-formation transition structure (**TS13**) (Table 4).

Case 1 yields differ notably from those previously reported by Zhang and co-workers.[13,14] The most obvious difference is that the previous study did not take into account the possibility of dioxole formation. Another key difference is that we have included all possible interconversions among the carbonyl oxides, while the previous study treated the reactions of the four carbonyl oxide conformers separately. If we did not allow for the possibility of interconversion, then dioxole formation would be far less important, since the only dioxole precursor is conformer **7d**. We explored this point quantitatively by performing two other sets of simulations (case 2 and case 3, Table 5).

In case 2, we removed all possible interconversions (reactions 5, 6, 9, and 10). This lowers the dioxole yield to 0.25 and substantially increases the yields of both dioxirane and collisionally stabilized **7**. More specifically, the yield of thermalized **7b** increases to 0.12, and the yield of thermalized **7c** increases to 0.10. In the full simulation (case 1), most of **7b** and **7c** convert to dioxole precursor **7d**, since the **7b ↔ 7d** and **7c ↔ 7d** interconversion barriers are (rather) low.

Methyl Vinyl Carbonyl Oxides

J. Phys. Chem. A, Vol. 109, No. 47, 2005 **10721**
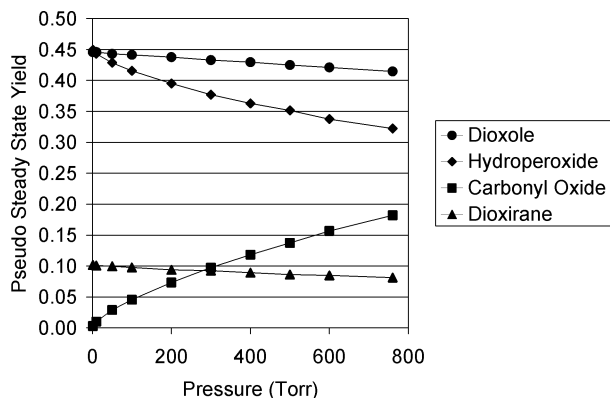
Figure 6. Pressure dependence of the total yields of dioxole (**16**), vinyl hydroperoxide (**14a**, **14b**, and **14c**), collisionally stabilized carbonyl oxide (**7a**, **7b**, **7c**, and **7d**), and dioxirane (**15a** and **15b**).

In case 3, we allowed for rotation about the $C_\beta-C_\gamma$ single bonds (reactions 5 and 6) but still forbade rotation about the $C_\gamma=O_\alpha$ double bonds (reactions 9 and 10). In this simulation, the dioxole yield (0.36) is close to the yield (0.42) in the unaltered simulation, case 1. The remaining 0.06 of dioxole yield must come from the rotation about the $C_\gamma=O_\alpha$ bond in **7a** and **7b**. While rotation about C=O is certainly the slowest process in our mechanism, a significant fraction of the methyl vinyl carbonyl oxide is formed with internal energy about the barriers for C=O rotation and our simulations demonstrate that rotation about C=O has a nonnegligible effect on product branching ratios.

Finally, in case 4, we address the possibility that our CBS-QB3 calculations systematically underestimate hydrogen-shift reaction barriers. We performed the same set of simulations as in case 1, except that we raised the energy of each of the three hydrogen-shift transition structures (**TS11a**, **TS11b**, and **TS11c** in Scheme 14) by 1.0 kcal/mol. With these adjustments, our predicted hydroperoxide yield (0.24) is close to the prediction of Zhang and co-workers.[14] Our predicted overall yields of stabilized carbonyl oxide (0.24) and dioxirane (0.10) are both significantly lower than those predicted by Zhang and co-workers, since dioxole formation is still the most important exit channel.

Figure 6 shows the variation with pressure of the pseudo-steady-state yields for each of the categories of products. In general, the yields of the rearrangement products all decrease with pressure, as expected. However, the decrease in hydroperoxide formation is far steeper than the decrease in either dioxole or dioxirane formation. Most of the decrease in hydroperoxide yield, and most of the corresponding increase in stabilized carbonyl oxide yield, is due to the chemistry of

species **7a** (data not shown). The significance of this pressure dependence is discussed in the next section.

The pseudo-steady-state yields reported in Table 5 and Figure 6 will be sensitive to our assumptions regarding the average energy transferred per collision ($\langle E_d \rangle$) and how the energy released by primary ozonide formation is partitioned between internal and external degrees of freedom (cf. Scheme 16). In their computational study of dimethyl carbonyl oxide, Kroll et al.[94] reported the impact of these two assumptions on hydroperoxide yield. They found that the prompt hydroperoxide yield decreases significantly with increasing pressure even when $\langle E_d \rangle$ was assumed to be as low as 100 cm^{-1}. With regard to energy partitioning, it is likely that assuming that only the energy in excess of the cycloreversion barrier can partition into the carbonyl oxides' internal degrees of freedom underestimates the extent of chemical activation. Kroll et al. predicted that a 10 kcal/mol increase in the activation of dimethyl carbonyl oxide more than doubles the 1-atm prompt yield of hydroperoxide. It is reasonable to assume that our predicted hydroperoxide yields will exhibit similar sensitivity to these parameter changes.

F. Subsequent Chemistry and Atmospheric Significance of the Isomerization Products. (1) Dioxoles. Like their methyl vinyl carbonyl oxide precursors, each of the rearrangement products is chemically activated and is expected to undergo further unimolecular rearrangement and/or decomposition. We explored this quantitatively for the 5-methyl-1,2-dioxole **16**. Scheme 17 shows the lowest barrier pathways available to the dioxole; each structure is labeled with its CBS-QB3 energy relative to that of **16**. Figure 7 shows the optimized structures obtained for each of these species (besides **16**).

Like dioxiranes,[108] the isomerization of **16** is initiated by the homolysis of the weak $O_\alpha-O_\beta$ bond. The barrier to homolysis is predicted to be 20.7 kcal/mol. In **TS17**, the $C_\gamma-O_\alpha$ and $C_\alpha-O_\beta$ bonds are both 0.07 Å shorter than the corresponding bonds in **16** (Figure 5), suggesting the presence in **TS17** of (hyper)-conjugation to the incipient radical centers on O_α and O_β. The most stable conformer of the 1,3-diradical product **18** is only 2.5 kcal/mol higher in energy than **16**. The diradical is stabilized by the vinoxy-like delocalization of the unpaired electron between C_β and O_α. Species **18**'s rather short $C_\gamma-O_\alpha$ bond (1.232 Å) and rather long $C_\beta-C_\gamma$ bond (1.448 Å) are consistent with a C_β-centered radical.

The diradical can undergo two rearrangements to form closed-shell structures. Reaction 21 involves ring closure (via **TS19**) to form the 1,2-epoxy-3-butanone (**21**). The reaction barrier is only 1.9 kcal/mol, and the reaction energy is −46.7 kcal/mol. As expected for an strongly exothermic reaction, the transition structure is early: the O_β-C_β distance is only 0.15 Å shorter in **TS19** than in **18**, while the same distance is 1.01 Å shorter in **21** than in **18**. The other possible rearrangement, reaction 22,

SCHEME 17
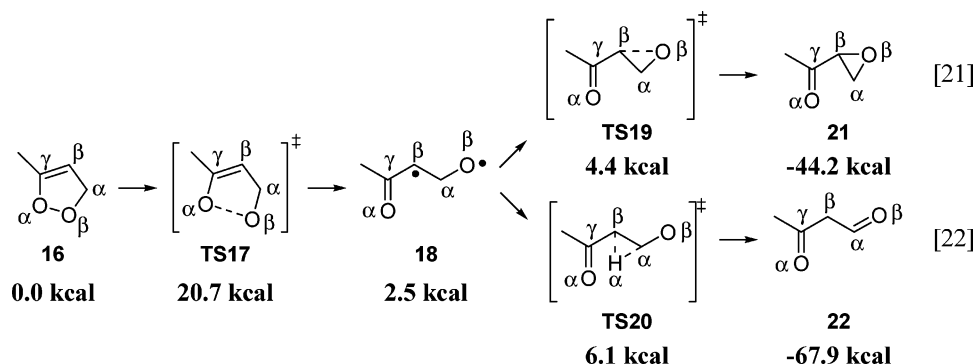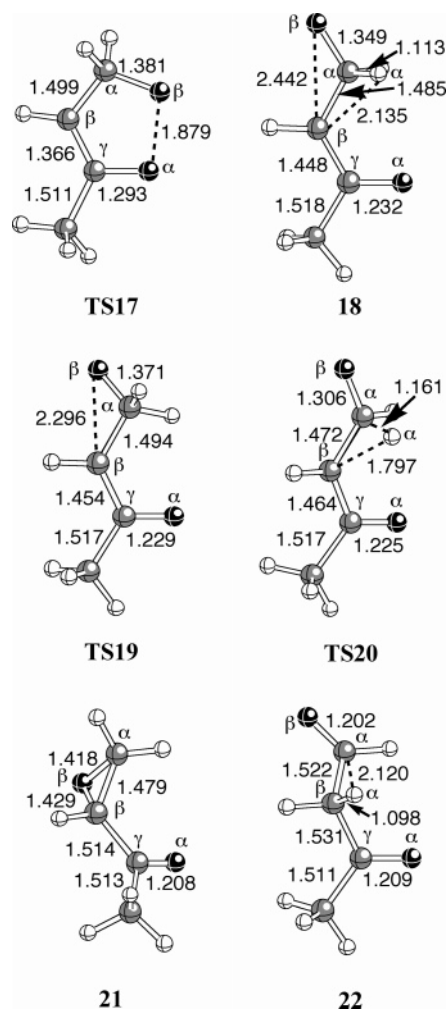
Figure 7. Optimized geometries for the structures in Scheme 17. Bond lengths (in angstroms) obtained at the B3LYP/6-311G(2d,d,p) level.

is a 1,2-hydrogen shift (via **TS20**) to form 3-oxobutanal (**22**). The reaction barrier is 3.6 kcal/mol, and the reaction energy is −70.4 kcal/mol. Again, as expected, the transition structure is rather early: the $H_\alpha-C_\beta$ distance is only 0.34 Å shorter in **TS20** than in **18**, while the same distance is 1.04 Å shorter in **22** than in **18**.

To estimate the yields of epoxide and dicarbonyl from methyl vinyl carbonyl oxide, we performed a set of master equation simulations (case 6) that included all the reactions in case 1 (as discussed in section IIIE), plus the reactions in Scheme 17. Thus, in case 6, dioxole **16** is treated as a well, not as an exit channel. The key results from these simulations are as follows: (1) The yield of each hydroperoxide exit channel, dioxirane exit channel, and stabilized carbonyl oxide is identical to that computed for case 1 (see Table 5). This demonstrates that dioxole formation is irreversible. (2) Within the precision of our simulations, no dioxole is collisionally stabilized at pressures up to 1 atm. (3) The 1-atm yield of epoxide **21** is 0.25, and the 1-atm yield of dicarbonyl **22** is 0.17.

It is noteworthy that there is experimental evidence for the formation of these dioxole derivatives. Scarpati and co-workers,[104,105] in the same study in which they obtained spectroscopic evidence for the dioxole **C** (Scheme 15), also quantified dioxole rearrangement products (Scheme 18). With both phenyl and acetyl groups at the 3-position, the major product detected was epoxide **D** (reaction 23). With only an acetyl group at the 3-position, the major product detected was the 1,3-dicarbonyl **F** (reaction 24). Given both the computational

evidence presented here and precedence in experimental solution-phase studies, we propose that species **21** and **22** are both significant products of isoprene ozonolysis and should be detectable in both smog chamber studies and in the troposphere.

SCHEME 18
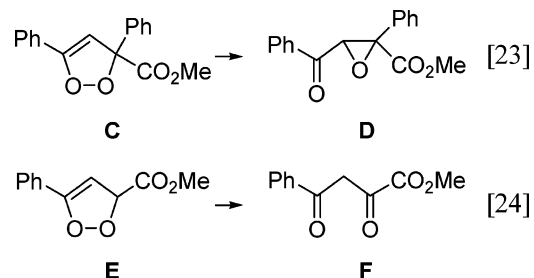
(2) Vinyl Hydroperoxides. It is well established that under atmospheric conditions, vinyl hydroperoxides **14a**−**c** will decompose promptly and quantitatively to form vinoxy and hydroxyl radicals (e.g., reaction 25).
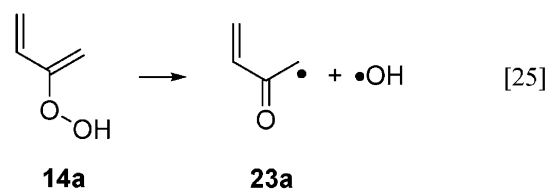
Vinoxy radical **23a** will react with O_2 to form an α-oxoperoxy radical. This species will likely thermalize before undergoing any intramolecular hydrogen shifts[56] and then undergo typical bimolecular reactions.[109,110]

Previous computational studies of isoprene ozonolysis[10,13,14] have assumed that the methyl vinyl carbonyl oxides **7** are the only sources of ·OH. If we assume the branching ratios predicted by Zhang and Zhang[13] for the cycloaddition of O_3 to isoprene, then we can estimate the overall ·OH yield predicted by our simulations. As discussed in section IIIB, Zhang and Zhang's branching ratio for the 1,2-primary ozonide (**4**) is 0.59. The total yield of **7** from **4** is 0.72 (Table 2). The total yield of **14** from **7** is 0.32 (Table 5, case 1). The prompt ·OH yield is therefore (0.59)(0.72)(0.32) = 0.14. This is significantly lower than all recent experimental measurements of ·OH yield,[6,21,24,25−28] although slightly higher than the prompt ·OH yield predicted by Zhang and co-workers.[13,14] However, as noted in section IIIE, our master equation simulations may have underestimated the chemical activation of **7**. Higher activation would lead to a higher yield of **14** (at the expense of thermalized **7**) and hence a predicted prompt ·OH yield in better agreement with experiment.

There are at least two other possible ·OH sources in isoprene ozonolysis. One is the 1,4-hydrogen shift within thermalized **7a** and **7b**. Transition state theory calculations by Zhang and co-workers[14] predict that with respect to unimolecular reactions, thermalized **7a** and **7b** will exclusively form vinyl hydroperoxides, which in turn decompose to give ·OH. Moreover, Kroll et al.[6,94] have provided both experimental and computational evidence that a significant fraction of the ·OH measured in smog chamber experiments will come from the thermal reaction of *syn*-alkyl carbonyl oxides. Including the putative contribution from thermalized **7a** and **7b** (yields in Table 5) increases our predicted ·OH yield to (0.59)(0.72)(0.32 + 0.14 + 0.01) = 0.20, which does agree (within the uncertainties) with most recent measurements.[24−26,28] Zhang and

Methyl Vinyl Carbonyl Oxides

J. Phys. Chem. A, Vol. 109, No. 47, 2005 **10723**

co-workers[13,14] predict a prompt + thermalized •OH yield of 0.25, which is in closer agreement to experiment.

If we were to assume that CBS-QB3 underestimates hydrogen-shift barriers in carbonyl oxides (Table 5, case 4), then we would predict a prompt •OH yield of $(0.59)(0.72)(0.24) = 0.10$ and a total •OH yield of $(0.59)(0.72)(0.24 + 0.19 + 0.02) = 0.19$. Again, the total predicted •OH yield would fall within the uncertainties of most recent measurements.

However, given the rather long lifetime of thermalized methyl vinyl carbonyl oxides with respect to unimolecular reaction ($\sim$15 s),[14] it is possible that in the troposphere, these species may preferentially undergo bimolecular reactions with species such as H_2O.[20,111−113] Recent experimental and computational studies[30,57] suggest that the α-hydroxy hydroperoxides formed in the H_2O reaction cannot subsequently decompose to afford •OH under atmospheric conditions.

A second possible •OH source is formaldehyde oxide **8**. Donahue and co-workers[6,94,114] have presented evidence that a significant fraction of **8** isomerizes promptly, first to the dioxirane and then to formic acid (HCOOH). The large exothermicity of HCOOH formation, in turn, drives the acid's prompt decomposition to HCO• and •OH. The decomposition of the "hot" acid may account for the 0.15 •OH yield[91] in ethene ozonolysis (at 1 atm). Zhang and co-workers[14] predicted that the total yield of **8** from isoprene ozonolysis is 0.33. If the **8** formed from isoprene behaved similarly to the **8** formed from ethene, then we would expect **8** to contribute 0.05 to the total •OH yield, improving the agreement between theory and experiment. However, in isoprene ozonolysis the majority of the energy released upon primary ozonide formation and cycloreversion will partition into the larger co-generated MVK (**9**) or methacrolein (**9′**) (Scheme 1). It is therefore not clear if 15% of **8** possesses enough energy to close to the dioxirane and ultimately form •OH.

Our simulations predict a significant decrease in the prompt yield of **14**, and therefore a decrease in the prompt yield of •OH, with increasing pressure (Figure 6). As noted in section IIIE, this pressure dependence is rather insensitive to changes in the $\langle E_d \rangle$ parameter. The predicted trend, but not the magnitude, in prompt •OH is consistent with the LIF measurements of Kroll et al.,[6,94] whose experiments probe •OH on a short ($\sim$10 ms) time scale. As discussed in section IIIE, virtually all of the **14** that would have been formed at low pressure instead results in thermalized **7a**. Our simulations therefore predict no pressure dependence in •OH yield on the longer time scale probed by scavenger experiments *if* thermalized **7a** also forms •OH.

(3) Dioxiranes. A variety of products may come from the isomerization and decomposition of the chemically activated dioxiranes **15a** and **15b**. Experimental studies of isoprene ozonolysis[11,115] and computational studies on smaller dioxiranes[108,116] strongly suggest that some fraction of **15** fragments into propene and CO_2 via a diradical intermediate like **24b** (reaction 26).
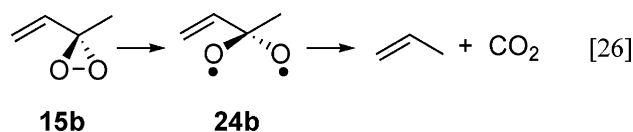
Fan and Zhang[117] have recently suggested that **15b** (or **24b**) may also lose or donate atomic oxygen to form MVK.

IV. Conclusions

We have used quantum chemistry and RRKM/master equation calculations to characterize the effect of the vinyl group

on the chemistry of the methyl vinyl carbonyl oxide. The vinyl group (a) lowers the barrier to rotation about the C=O bond and (b) allows the carbonyl oxide to cyclize to a dioxole. Our calculations predict that these two effects work together to make dioxole formation the most important reaction pathway for the methyl vinyl carbonyl oxide. The rearrangement products of the dioxole, 1,2-epoxy-3-butanone and 3-oxobutanal, should be major products of isoprene ozonolysis. Calculations in progress in our laboratory seek to quantify the yields of the analogous products from the ozonolysis of the 3,4-double bond of isoprene.

More generally, our simulations of both primary ozonide cycloreversion and carbonyl oxide isomerization demonstrate the importance of treating all energetically accessible reaction pathways in master equation simulations. This has implications for modeling the chemistry of cycloalkene-derived carbonyl oxides. Since these species do not fragment upon cycloreversion, they retain all the energy released by primary ozonide formation and can undergo unimolecular reactions not accessible to thermalized or only moderately chemically activated intermediates.[99]

The calculations reported here, combined with Zhang and co-workers' treatment of isoprene ozonolysis kinetics,[13,14] allow us to estimate methyl vinyl ketone and •OH yields consistent with the majority of experimental measurements. Nevertheless, additional theoretical and experimental studies are still needed to characterize the ability of isoprene-derived formaldehyde oxide and thermalized carbonyl oxides to afford •OH.

Supporting Information Available: Cartesian coordinates of all labeled minima and transition structures presented in this paper. This material is available free of charge via the Internet at http://pubs.acs.org.

References and Notes

(1) Guenther, A.; Hewitt, C. N.; Erickson, D.; Fall, R.; Geron, C.; Graedel, T.; Harley, P.; Klinger, L.; Lerdau, M.; McKay, W. A.; Pierce, T.; Scholes, B.; Steinbrecher, R.; Tallamraju, R.; Taylor, J.; Zimmerman, P. *J. Geophys. Res.* **1995**, *100*, 8873.

(2) Atkinson, R.; Arey, J. *Chem. Rev.* **2003**, *103*, 4605.

(3) Atkinson, R.; Arey, J. *Atmos. Environ.* **2003**, *37*, S197.

(4) Atkinson, R.; Arey, J. *Acc. Chem. Res.* **1998**, *31*, 574.

(5) Paulson, S. E.; Orlando, J. J. *Geophys. Res. Lett.* **1996**, *23*, 3727.

(6) Kroll, J. H.; Hanisco, T. F.; Donahue, N. M.; Demerjian, K. L.; Anderson, J. G. *Geophys. Res. Lett.* **2001**, *28*, 3863.

(7) Hu, J.; Stedman, D. H. *Environ. Sci. Technol.* **1995**, *29*, 1655.

(8) Heard, D. E.; Pilling, M. J. *Chem. Rev.* **2003**, *103*, 5163.

(9) Anglada, J. M.; Bofill, J. M.; Olivella, S.; Solé, A. *J. Am. Chem. Soc.* **1996**, *118*, 4636.

(10) Gutbrod, R.; Kraka, E.; Schindler, R. N.; Cremer, D. *J. Am. Chem. Soc.* **1997**, *119*, 7330.

(11) Paulson, S. E.; Flagan, R. C.; Seinfeld, J. H. *Int. J. Chem. Kinet.* **1992**, *24*, 103.

(12) Aschmann, S. M.; Atkinson, R. *Environ. Sci. Technol.* **1994**, *28*, 1539.

(13) Zhang, D.; Zhang, R. *J. Am. Chem. Soc.* **2002**, *124*, 2692.

(14) Zhang, D.; Lei, W.; Zhang, R. *Chem. Phys. Lett.* **2002**, *358*, 171.

(15) Atkinson, R. *J. Phys. Chem. Ref. Data* **1997**, *26*, 215.

(16) Khamaganov, V. G.; Hites, R. A. *J. Phys. Chem. A* **2001**, *105*, 815.

(17) Avzianova, E. V.; Ariya, P. A. *Int. J. Chem. Kinet.* **2002**, *34*, 678.

(18) Klawatsch-Carrasco, N.; Doussin, J. F.; Carlier, P. *Int. J. Chem. Kinet.* **2004**, *36*, 152.

(19) Orzechowska, G.; Paulson, S. E. *J. Phys. Chem. A* **2005**, *109*, 5358.

(20) Hasson, A. S.; Ho, A. W.; Kuwata, K. T.; Paulson, S. E. *J. Geophys. Res.* **2001**, *106*, 34143.

(21) Rickard, A. R.; Johnson, D.; McGill, C. D.; Marston, G. *J. Phys. Chem. A* **1999**, *103*, 7656.

(22) Sauer, F.; Schäfer, C.; Neeb, P.; Horie, O.; Moortgat, G. K. *Atmos. Envir.* **1999**, *33*, 229.

(23) Grosjean, D.; Williams, E. L., II; Grosjean, E. *Environ. Sci. Technol.* **1993**, *27*, 830.

(24) Atkinson, R.; Aschmann, S. M.; Arey, J.; Shorees, B. *J. Geophys. Res.* **1992**, *97*, 6065.

(25) Paulson, S. E.; Chung, M.; Sen, A. D.; Orzechowska, G. *J. Geophys. Res.* **1998**, *103*, 25533.

(26) Neeb, P.; Moortgat, G. K. *J. Phys. Chem. A* **1999**, *103*, 9003.

(27) Lewin, A. G.; Johnson, D.; Price, D. W.; Marston, G. *Phys. Chem. Chem. Phys.* **2001**, *3*, 1253.

(28) Gutbrod, R.; Meyer, S.; Rahman, M. M.; Schindler, R. N. *Int. J. Chem. Kinet.* **1997**, *29*, 717.

(29) Vereecken, L.; Peeters, J. *J. Phys. Chem. A* **2004**, *108*, 5197.

(30) Aplincourt, P.; Anglada, J. M. *J. Phys. Chem. A* **2003**, *107*, 5798.

(31) Frisch, M. J.; Trucks, G. W.; Schlegel, H. B.; Scuseria, G. E.; Robb, M. A.; Cheeseman, J. R.; J. A. Montgomery, J.; Vreven, T.; Kudin, K. N.; Burant, J. C.; Millam, J. M.; Iyengar, S. S.; Tomasi, J.; Barone, V.; Mennucci, B.; Cossi, M.; Scalmani, G.; Rega, N.; Petersson, G. A.; Nakatsuji, H.; Hada, M.; Ehara, M.; Toyota, K.; Fukuda, R.; Hasegawa, J.; Ishida, M.; Nakajima, T.; Honda, Y.; Kitao, O.; Nakai, H.; Klene, M.; Li, X.; Knox, J. E.; Hratchian, H. P.; Cross, J. B.; Adamo, C.; Jaramillo, J.; Gomperts, R.; Stratmann, R. E.; Yazyev, O.; Austin, A. J.; Cammi, R.; Pomelli, C.; Ochterski, J. W.; Ayala, P. Y.; Morokuma, K.; Voth, G. A.; Salvador, P.; Dannenberg, J. J.; Zakrzewski, V. G.; Dapprich, S.; Daniels, A. D.; Strain, M. C.; Farkas, O.; Malick, D. K.; Rabuck, A. D.; Raghavachari, K.; Foresman, J. B.; Ortiz, J. V.; Cui, Q.; Baboul, A. G.; Clifford, S.; Cioslowski, J.; Stefanov, B. B.; Liu, G.; Liashenko, A.; Piskorz, P.; Komaromi, I.; Martin, R. L.; Fox, D. J.; Keith, T.; Al-Laham, M. A.; Peng, C. Y.; Nanayakkara, A.; Challacombe, M.; Gill, P. M. W.; Johnson, B.; Chen, W.; Wong, M. W.; Gonzalez, C.; Pople, J. A. *Gaussian 03*, revision B.05; Gaussian Inc.: Pittsburgh, PA, 2003.

(32) Becke, A. D. *J. Chem. Phys.* **1993**, *98*, 5648.

(33) Stephens, P. J.; Devlin, F. J.; Chabalowski, C. F.; Frisch, M. J. *J. Phys. Chem.* **1994**, *98*, 11623.

(34) Hehre, W. J.; Ditchfield, R.; Pople, J. A. *J. Chem. Phys.* **1972**, *56*, 2257.

(35) Hariharan, P. C.; Pople, J. A. *Theor. Chim. Acta* **1973**, *28*, 213.

(36) Gonzalez, C.; Schlegel, H. B. *J. Phys. Chem.* **1990**, *94*, 5523.

(37) Gonzalez, C.; Schlegel, H. B. *J. Chem. Phys.* **1989**, *90*, 2154.

(38) Coote, M. L. *J. Phys. Chem. A* **2004**, *108*, 3865.

(39) Lynch, B. J.; Fast, P. L.; Harris, M.; Truhlar, D. G. *J. Phys. Chem. A* **2000**, *104*, 4811.

(40) Lynch, B. J.; Truhlar, D. G. *J. Phys. Chem. A* **2001**, *105*, 2936.

(41) Zhao, Y.; Pu, J.; Lynch, B. J.; Truhlar, D. G. *Phys. Chem. Chem. Phys.* **2004**, *6*, 673.

(42) Jursic, B. S. *J. Mol. Struct. (THEOCHEM)* **1998**, *430*, 17.

(43) Malick, D. K.; Petersson, G. A.; Montgomery, J. A., Jr. *J. Chem. Phys.* **1998**, *108*, 5704.

(44) Kuwata, K. T.; Templeton, K. L.; Hasson, A. S. *J. Phys. Chem. A* **2003**, *107*, 11525.

(45) Montgomery, J. A., Jr.; Frisch, M. J.; Ochterski, J. W.; Petersson, G. A. *J. Chem. Phys.* **1999**, *110*, 2822.

(46) Bartlett, R. J. *J. Phys. Chem.* **1989**, *93*, 1697.

(47) Wijaya, C. D.; Sumathi, R.; Green, W. H., Jr. *J. Phys. Chem. A* **2003**, *107*, 4908.

(48) Glendening, E. D.; J, K. B.; Reed, A. E.; Carpenter, J. E.; Bohmann, J. A.; Morales, C. M.; Weinhold, F. *NBO 5.0*; University of Wisconsin: Madison, WI, 2001.

(49) Reed, A. E.; Weinstock, R. B.; Weinhold, F. *J. Chem. Phys.* **1985**, *83*, 735.

(50) Glendening, E. D.; Weinhold, F. *J. Comput. Chem.* **1998**, *19*, 593.

(51) Glendening, E. D.; Weinhold, F. *J. Comput. Chem.* **1998**, *19*, 610.

(52) Glendening, E. D.; Badenhoop, J. K.; Weinhold, F. *J. Comput. Chem.* **1998**, *19*, 628.

(53) Gomez-Balderas, R.; Coote, M. L.; Henry, D. J.; Radom, L. *J. Phys. Chem. A* **2004**, *108*, 2874.

(54) Henry, D. J.; Parkinson, C. J.; Radom, L. *J. Phys. Chem. A* **2002**, *106*, 7927.

(55) Guner, V.; Khuong, K. S.; Leach, A. G.; Lee, P. S.; Bartberger, M. D.; Houk, K. N. *J. Phys. Chem. A* **2003**, *107*, 11445.

(56) Kuwata, K. T.; Hasson, A. S.; Dickinson, R. V.; Petersen, E. B.; Valin, L. C. *J. Phys. Chem. A* **2005**, *109*, 2514.

(57) Hasson, A. S.; Chung, M. Y.; Kuwata, K. T.; Converse, A. D.; Krohn, D.; Paulson, S. E. *J. Phys. Chem. A* **2003**, *107*, 6176.

(58) Zhang, D.; Zhang, R. *J. Chem. Phys.* **2005**, *122*, 114308.

(59) Lei, W.; Derecskei-Kovacs, A.; Zhang, R. *J. Chem. Phys.* **2000**, *113*, 5354.

(60) Martin, J. M. L.; Oliveira, G. D. *J. Chem. Phys.* **1999**, *111*, 1843.

(61) Bach, R. D.; Andres, J. L.; Owensby, A. L.; Schlegel, H. B.; McDouall, J. J. W. *J. Am. Chem. Soc.* **1992**, *114*, 7207.

(62) Wesolowski, T. A.; Parisel, O.; Ellinger, Y.; Weber, J. *J. Phys. Chem. A* **1997**, *101*, 7818.

(63) Kohn, W.; Meir, Y.; Makarov, D. E. *Phys. Rev. Lett.* **1998**, *80*, 4153.

(64) van Mourik, T.; Gdanitz, R. J. *J. Chem. Phys.* **2002**, *116*, 9620.

(65) Tsuzuki, S.; Uchimaru, T.; Tanabe, K. *Chem. Phys. Lett.* **1998**, *287*, 202.

(66) Couronne, O.; Ellinger, Y. *Chem. Phys. Lett.* **1999**, *306*, 71.

(67) Kuczkowski, R. L. *Chem. Soc. Rev.* **1992**, 79.

(68) Gillies, C. W.; Gillies, J. Z.; Suenram, R. D.; Lovas, F. J.; Kraka, E.; Cremer, D. *J. Am. Chem. Soc.* **1991**, *113*, 2412.

(69) Ljubic, I.; Sabljic, A. *J. Phys. Chem. A* **2002**, *106*, 4745.

(70) Zhao, Y.; Truhlar, D. G. *J. Phys. Chem. A* **2004**, *108*, 6908.

(71) Lynch, B. J.; Zhao, Y.; Truhlar, D. G. *J. Phys. Chem. A* **2003**, *107*, 1384.

(72) Barker, J. R. *MultiWell*, 1.3.2 ed.; University of Michigan: Ann Arbor, MI, July, 2003.

(73) Barker, J. R. *Int. J. Chem. Kinet.* **2001**, *33*, 232.

(74) Robinson, P. J.; Holbrook, K. A. *Unimolecular Reactions*; Wiley-Interscience: London, 1972.

(75) Ayala, P. Y.; Schlegel, H. B. *J. Chem. Phys.* **1998**, *108*, 2314.

(76) Barker, J. R.; Ortiz, N. F. *Int. J. Chem. Kinet.* **2001**, *33*, 246.

(77) Barker, J. R.; Yoder, L. M.; King, K. D. *J. Phys. Chem. A* **2001**, *105*, 796.

(78) Mourits, F. M.; Rummens, F. H. A. *Can. J. Chem.* **1977**, *55*, 3007.

(79) Hippler, H.; Troe, J.; Wendelken, H. J. *J. Chem. Phys.* **1983**, *78*, 6709.

(80) McCann, D. W.; Danner, R. P. *Ind. Eng. Chem. Process Des. Dev.* **1984**, *23*, 529.

(81) Joback, K. G.; Reid, R. C. *Chem. Eng. Comm.* **1987**, *57*, 233.

(82) Reid, R. C.; Prausnitz, J. M.; Poling, B. E. *The Properties of Gases and Liquids*; McGraw-Hill: New York, 1987.

(83) Dean, J. A. *Lange's Handbook of Chemistry*, 14th ed.; McGraw-Hill: New York, 1992.

(84) Hirschfelder, J. O.; Curtiss, C. F.; Bird, R. B. *Molecular Theory of Gases and Liquids*; Wiley: New York, 1954.

(85) Snider, N. *J. Chem. Phys.* **1984**, *80*, 1885.

(86) Muller, N.; Falk, A. *Ball & Stick 3.8b3, Molecular Graphics Software for MacOS*; Johannes Kepler University: Linz, Austria, 2000.

(87) Olzmann, M.; Kraka, E.; Cremer, D.; Gutbrod, R.; Andersson, S. *J. Phys. Chem. A* **1997**, *101*, 9421.

(88) Chan, W.-T.; Hamilton, I. P. *J. Chem. Phys.* **2003**, *118*, 1688.

(89) Ljubic, I.; Sabljic, A. *J. Phys. Chem. A* **2002**, *106*, 4745.

(90) Anglada, J. M.; Crehuet, R.; Bofill, J. M. *Chem.−Eur. J.* **1999**, *5*, 1809.

(91) It should also be noted that there is some evidence for the stepwise decomposition of the primary ozonide (Fenske, J. D.; Hasson, A. S.; Paulson, S. E.; Kuwata, K. T.; Ho, A.; Houk, K. N. *J. Phys. Chem. A* **2000**, *104*, 7821; Fajgar, R.; Roithova, J.; Pola, J. *J. Org. Chem.* **2001**, *66*, 6977). This pathway would be initiated by the homolysis of one of the weak O−O bonds. The resulting oxy/peroxy diradical could then eliminate O_2 and form an epoxide. Atkinson et al. (Atkinson, R.; Arey, J.; Aschmann, S. M.; Tuazon, E. C. *Res. Chem. Intermed.* **1994**, *20*, 385) measure a ∼1% yield of the epoxide derived from the 1,2-primary ozonide.

(92) Wiberg, K. B.; Hadad, C. M.; Rablen, P. R.; Cioslowski, J. *J. Am. Chem. Soc.* **1992**, *114*, 8644.

(93) Wadt, W. R.; Goddard, W. A., III. *J. Am. Chem. Soc.* **1975**, *97*, 3004.

(94) Kroll, J. H.; Sahay, S. R.; Anderson, J. G.; Demerjian, K. L.; Donahue, N. M. *J. Phys. Chem. A* **2001**, *105*, 4446.

(95) Cremer, D. *J. Am. Chem. Soc.* **1979**, *101*, 7199.

(96) Loncharich, R. J.; Brown, F. K.; Houk, K. N. *J. Org. Chem.* **1989**, *54*, 1129.

(97) Fenske, J. D.; Kuwata, K. T.; Houk, K. N.; Paulson, S. E. *J. Phys. Chem. A* **2000**, *104*, 7246.

(98) Rathman, W. C. D.; Claxton, T. A.; Rickard, A. R.; Marston, G. *Phys. Chem. Chem. Phys.* **1999**, *1*, 3981.

(99) Chuong, B.; Zhang, J.; Donahue, N. M. *J. Am. Chem. Soc.* **2004**, *126*, 12363.

(100) Cremer, D.; Schmidt, T.; Gauss, J.; Radhakrishnan, T. P. *Angew. Chem., Int. Ed. Engl.* **1988**, *27*, 427.

(101) Huisgen, R. *Angew. Chem., Int. Ed. Engl.* **1980**, *19*, 947.

Methyl Vinyl Carbonyl Oxides

J. Phys. Chem. A, Vol. 109, No. 47, 2005 **10725**

(102) Fabian, W. M. F.; Bakulev, V. A.; Kappe, C. O. *J. Org. Chem.* **1998**, *63*, 5801.

(103) Fabian, W. M. F.; Kappe, C. O.; Bakulev, V. A. *J. Org. Chem.* **2000**, *65*, 47.

(104) Graziano, M. L.; Iesce, M. R.; Cermola, F.; Cimminiello, G.; Scarpati, R. *J. Chem. Soc., Perkin Trans. 1* **1991**, 1479.

(105) Graziano, M. L.; Iesce, M. R.; Cimminiello, G.; Scarpati, R. *J. Chem. Soc., Perkin Trans. 1* **1989**, 241.

(106) Aitken, R. A.; Hill, L. 1,2-Dioxoles and 1,2-Oxathioles. In *Comprehensive Heterocyclic Chemistry II*; Katritzky, A. R., Rees, C. W., Scriven, E. F. V., Shinkai, I., Eds.; Pergamon Press: Oxford, U.K., 1996; Vol. 3, p 511.

(107) Forst, W. *Theory of Unimolecular Reactions*; Academic Press: New York, 1972.

(108) Cremer, D.; Kraka, E.; Szalay, P. G. *Chem. Phys. Lett.* **1998**, *292*, 97.

(109) Kirchner, F.; Stockwell, W. R. *J. Geophys. Res.* **1996**, *101*, 21007.

(110) Tyndall, G. S.; Cox, R. A.; Granier, C.; Lesclaux, R.; Moortgat, G. K.; Pilling, M. J.; Ravishankara, A. R.; Wallington, T. J. *J. Geophys. Res.* **2001**, *106*, 12157.

(111) Hatakeyama, S.; Lai, H.; Gao, S.; Murano, K. *Chem. Lett.* **1993**, 1287.

(112) Horie, O.; Moortgat, G. K. *Acc. Chem. Res.* **1998**, *31*, 387.

(113) Hasson, A. S.; Orzechowska, G.; Paulson, S. E. *J. Geophys. Res.* **2001**, *106*, 34131.

(114) Donahue, N. M.; Kroll, J. H.; Anderson, J. G.; Demerjian, K. L. *Geophys. Res. Lett.* **1998**, *25*, 59.

(115) Carter, W. P. L.; Atkinson, R. *Int. J. Chem. Kinet.* **1996**, *28*, 497.

(116) Anglada, J. M.; Bofill, J. M.; Olivella, S.; Sole, A. *J. Phys. Chem. A* **1998**, *102*, 3398.

(117) Fan, J.; Zhang, R. *Environ. Chem.* **2004**, *1*, 140.